Mutations in specific MT5-MMP domains prevent the accumulation of toxic APP metabolites and serve as templates for peptide-based therapeutics in cell models of Alzheimer's disease

Pedro Belio-Mairal[1a], Athina Kamitsou A[1], Delphine Stephan D[1], Nicolas Jullien[1], Diarra Thianeq[1], Melissa Ramos M[1], Laurence Louis[1], Florian Benoist[2], Bastien Serrano[2], Marion David[2], Michel Khrestchatisky[1], Pascaline Lécorché[2], Emmanuel Nivet E[1], Santiago Rivera[1]*.

1. Aix-Marseille Univ, CNRS, INP, Inst Neurophysiopathol, Marseille, France

2. Vect-Horus S.A.S., Faculté de Médecine, Marseille, France

a. Present address: Quantitative Bioscience Institute, University of California, San Francisco, California, USA

* Corresponding author, santiago.rivera@univ-amu.fr

Institute of Neuropathophysiology (INP)
UMR 7051, CNRS - Aix-Marseille Université
Campus Timone
27 Bld Jean Moulin
13005 Marseille
France
Tel: 33 4 91 69 87 71
Tel: 33 4 91 69 89 64
Fax: 33 4 91 25 89 70

ABSTRACT

In previous works we identified a key role for membrane-type 5-matrix metalloproteinase (MT5-MMP) in Alzheimer's disease (AD) pathogenesis. We demonstrated the involvement of the C-terminal transmembrane (TM) and intracellular (IC) domains of the proteinase in the fate of major toxic metabolites of the amyloid precursor protein (APP) (*e.g.,* C99, Aβ). These findings led us to hypothesize that modifying MT5-MMP C-terminal domains could serve as an effective strategy to modulate C99 and Aβ. To test this, here we generated MT5-MMP variants carrying amino acid deletions or substitutions in entire proteinase domains or in selected amino acid clusters in the IC domain. MT5-MMP variants were co-transfected into human cell lines accumulating C99, reminiscent of an AD setting. We identified mutations in the IC domain that induce C99 degradation and a decrease in Aβ levels, while other mutations have divergent effects on these APP metabolites. Furthermore, high content imaging revealed the importance of MT5-MMP IC modifications in regulating subcellular trafficking of C99 through the endomembrane system and its consequences for C99 processing. Proximity ligation assays also highlighted the importance of the IC domain in MT5-MMP colocalization and potential interaction with C99. In a translational effort, we synthetized and functionalized peptides that mimic the MT5-MMP IC domain and carry mutations that reduce C99 and/or Aβ levels. One of these peptides reduced C99 levels in an *in vitro* AD model. Overall, our study highlights the role of selected amino acids in the C-terminal domains of MT5-MMP as the basis for a better understanding of the proteinase's contribution to C99 and Aβ metabolism. Furthermore, this study provides new insights for designing MT5-MMP-based strategies against AD, exploiting the unique properties of specific mutations in MT5-MMP domains to prevent the accumulation of C99 and Aβ.

Keywords: matrix metalloproteinase, secretase, amyloid beta precursor protein, C99 processing, scavenger, subcellular trafficking

INTRODUCTION

Matrix metalloproteinases (MMPs) form a multigenic family of more than 20 endopeptidases that display a wide spectrum of biological activities[1]. Membrane-type 5-matrix metalloproteinase (MT5-MMP, also known as MMP-24 or η-secretase), is the only MMP primarily expressed in neural cells[2,3] and is involved in a number of physiological and pathological processes in the nervous system, including: synaptic plasticity, neural stem cell differentiation, post-lesion synaptic reorganization and axonal growth and regeneration[4,5]

The presence of MT5-MMP in amyloid plaques from Alzheimer's disease (AD) patients suggests its involvement in AD pathogenesis[2]. Consistent with this, MT5-MMP cleaved amyloid precursor protein (APP) in HEK cells[6] and murine primary neurons[7]. This was further highlighted *in vivo*, where MT5-MMP deficiency reduced APP processing in the 5xFAD mouse model of AD[8,9]. APP processing is central in the amyloid hypothesis of AD, as β-secretase cleavage generates the APP C-terminal fragment (CTF) C99, which γ-secretase further processes to release beta-amyloid (Aβ)[10]. Beyond APP metabolism, MT5-MMP deficiency also decreased neuroinflammatory mediators, glial reactivity, and preserved long-term potentiation (LTP) and cognitive functions in 5xFAD mice[8,9]. Conversely, MT5-MMP overexpression led to C99 and Aβ accumulation in HEK cells carrying the APP Swedish familial AD mutation (HEKswe)[8].

While Aβ attracts much of the attention in AD, there is growing evidence pointing to the critical role of earlier events. Accumulation of C99 precedes Aβ buildup in the 3xTg and 5xFAD mouse models of AD[11,12]. In humans, C99 accumulates in the brains of AD patients, where it correlates with neuronal vulnerability and cognitive impairment[13]. C99 accumulation leads to endolysosomal dysfunctions independently of Aβ in both mouse and human models, which may account for the early toxic effects of C99[11,14]. We recently reported that MT5-MMP also controls the metabolism of APP CTFs *via* both dependent and independent proteolytic mechanisms[4]. Notably, only MT5-MMP transmembrane (TM) and intracellular (IC) non-catalytic domains maintained high levels of C99 and Aβ in HEK cells overexpressing C99, and a mutant version of MT5-MMP with only these two domains coimmunoprecipitated with C99[4]. Therefore, MT5-MMP non-catalytic functions seem to have a key role in C99 processing.

In this study, we aimed at understanding the mechanisms by which non-catalytic domains of MT5-MMP domains regulate C99. Using molecular, cell biology, and structure-function approaches, we assessed the importance of specific amino acids in the TM and IC domains of MT5-MMP in controlling C99 and Aβ. Our findings provide new insights into the functional interactions between MT5-MMP and C99, laying a foundation for therapeutic strategies that modulate C99 and Aβ by harnessing the molecular properties of MT5-MMP.

MATERIALS AND METHODS

Plasmid constructs

All plasmids were constructed using a pcDNA3.1 backbone. The new plasmids used in this study (ΔEXT, TM1/IC5, TM5/IC1, all the mutated variants of TM/IC) (Fig. 1A, 2A) were generated by GeneArt (ThermoFisher Scientific). Constructs encoding other MT5-MMP variants (pcDNA, TM/IC, EXT/TM, EXT) and C99 or HA-C99 were produced, purified, and amplified as previously described[4].

Cell lines

HEK cells were maintained in DMEM Glutamax (61965026, ThermoFisher Scientific) supplemented with 10% fetal bovine serum (FBS) (A3160801, ThermoFisher Scientific) and 1% penicillin/streptomycin (15140122, ThermoFisher Scientific) (hereafter referred as HEK medium). For passaging, cells were washed with DPBS (14190094, ThermoFisher Scientific) and dissociated with 0.05% Trypsin-EDTA (25300054, ThermoFisher Scientific). HEK medium was added, cells were pipetted into single cells and replated with fresh HEK medium in a new flask, where Geneticin (10131027, ThermoFisher Scientific) was added at a 1:100 dilution.

hTERT-RPE1 cells were cultured using the same protocol as for HEK cells, but using DMEM/F12 (31331028, ThermoFisher Scientific) supplemented with 10% FBS and 1% penicillin/streptomycin. HBSS (14025050, ThermoFisher Scientific) was used for washing. In addition, 0.25% Trypsin-EDTA (25200056, ThermoFisher Scientific) was used for cell dissociation.

Transfections and treatments

Cells were transfected using JetPei® Polyplus (101000053, Sartorius). For 96-well plate (6055300, Revvity; 353072, Corning) format, reverse transfection was used and hTERT-RPE1were plated at $1 \cdot 10^4$ cells/well. For 6-well plates (353046, Corning), HEK cells were plated at $1.5 \cdot 10^6$ cells/well and the classical forward transfection was used. In both cases, the manufacturer's instructions were followed with the recommended volumes of transfection reagents and DNA quantities. Transfection of synthetic peptides were done together with DNA plasmids.

All proteinase and ATPase inhibitors (Table 1) were diluted in DMSO (D2650, Sigma-Aldrich) and added 15–17 h after transfection. After 20 h of treatment, cells were lysed and collected for experiments.

For free uptake experiments, conjugated peptides were added with fresh HEK media at corresponding concentrations 24 h after HA-C99 transfection and left for 48 h of treatment.

MTT test

After 48 h of cell transfection or peptide treatment, we evaluated cell viability using the 3-(4,5-dimethylthiazol-2yl)-2,5-diphenyl tetrazolium bromide (MTT) assay (M5655 Sigma-Aldrich). MTT was diluted in HEK medium and added to each well to a final concentration of 0.5 mg/mL for 3 h at 37°C and 5% CO_2. After incubation, the culture medium was removed and replaced with 100 µL of dimethyl sulfoxide (DMSO) (D2650, Sigma-Aldrich) to dissolve the formazan crystals formed in the mitochondria of living cells. The absorbance was measured in a multiwell plate reader. The data were calculated as the percentage of live cells = (transfected cell OD_{550}/control cell OD_{550}) x 100, after normalizing the values by column and row.

Protein quantification

A BCA assay kit (23225, ThermoFisher Scientific) was used following the manufacturer's instructions for the multiwell plate format. The samples for the standard curves

were obtained from a ready-to-use BSA standard kit (23208, ThermoFisher Scientific). All measurements were performed in two technical replicates. Absorbance was measured using a multiwell plate reader. The standard curve was calculated using the 4-parameter fit of MARS data analysis software version 2.10R3 (BMG Labtech). Concentrations were extrapolated using the same software.

Western Blot

Samples with 20 µg of protein were mixed with 2x Tris-Glycine (LC2676, ThermoFisher Scientific) or Tricine (LC1676, ThermoFisher Scientific) sample buffer and heated at 95°C for 5 min or 85°C for 20 min for small-sized (<20 kDa) target proteins.

We used a Mini gel tank system (A25977, ThermoFisher Scientific) and a Power Blotter Semi-dry Transfer system (PB0013, ThermoFisher Scientific). All products cited in this section were purchased from ThermoFisher Scientific unless otherwise stated. Novex 4-20% Tris-Glycine gels with 10 wells (XP04200BOX) or 15 wells (XP04205BOX) and Novex 16% Tricine gels with 10-well (EC6695BOX) or 15-well (EC66955BOX) formats were run following the manufacturer's instructions.

Gels were transferred into 0.45 µm nitrocellulose blotting membranes (10600002, Amersham). The stacks were transferred in Towbin buffer in the PowerBlotter and ran as per manufacturer's recommendations. Membranes were incubated in Ponceau solution (P7170, Sigma-Aldrich) for 30 sec and the signal measured using the Preview mode on a NineAllience 9.7 17.02 (UVITec). The membranes were then blocked for 1 h in blocking buffer consisting of 1x PBS (ET330-A, Euromedex) with 5%$_{m/v}$ powder milk and 0.2%$_{v/v}$ Tween20 (P1379, Sigma-Aldrich). The membranes were incubated with antibodies diluted 1:1000 (anti-actin antibodies were diluted 1:5000) in blocking buffer overnight at 4°C with agitation, then washed and incubated with HRP-conjugated secondary antibodies (1:1000) in blocking buffer for 1 h at room temperature (RT). Immunoreactive bands were visualized with ECL solution (RPN2106, Amersham) or ECL Prime solution (RPN2236, Amersham), using the chemiluminescence mode of the UVITec station, and semi-quantified using Fiji's tool "Plot lanes" from the "Gels" module[15]. The actin band values were used as normalizing control.

Immunocytochemistry

Cells were cultured in 96-well plates (6055300, Revvity) for high content screening microscopy (HCS). For sample fixation, PEM buffer was prepared to obtain a final solution of PIPES 80 mM (P1851, Sigma-Aldrich), $MgCl_2$ 2mM (M9272, Honeywell), and EGTA 5mM (E4378, Sigma-Aldrich) at pH 6.8 in ddH_2O. Then, paraformaldehyde (15714, Electron Microscopy Services) was diluted at $4\%_{v/v}$ in PEM with $4\%_{m/v}$ sucrose (S0389, Sigma-Aldrich) (fixation solution).

Culture media was removed from 96-well plates and then washed with 1x DPBS. After fixing with fixation solution for 10 min at RT, cells were washed 4 times with DPBS, then blocked and permeabilized for 1 h at RT with $3\%_{m/v}$ bovine serum albumin (BSA) (A7906, Sigma-Aldrich), 0.1% saponin (84510, Sigma-Aldrich), and 10% normal goat (005-000-121, Jackson ImmunoResearch) or donkey (017-000-121, Jackson ImmunoResearch) serum in 1x DPBS (block/per buffer). Primary antibodies were added to cells and incubated overnight at 4°C at the corresponding concentrations (Table 2). The next day, cells were washed with 1x DPBS and the Alexa Fluor secondary antibodies diluted in blocking/permeabilizing buffer (Table 2) incubated for 1 h at RT. After washing in 1x DPBS cells were incubated for 10 min at RT with 10 µg/mL Hoechst33342 (H3570, ThermoFisher Scientific) diluted in 1x DPBS. After washing twice with 1x DPBS, plates were sealed with parafilm and stored in 1xDPBS. Plates were imaged within 24 h.

Microscopy analyses

Python procedures to clean, downsize, normalize, and visualize quantitative data from the automated microscope were run in Jupyter Notebooks (available at: github.com/RiveraLabINP/BelioMairal_2024). In brief, the overlap values of individual cells were retrieved from the Operetta© software (quantification workflow available at: github.com/RiveraLabINP/BelioMairal_2024). These values were multiplied by the area of HA fluorescence to generate a new variable representing the total area of overlap of HA with each organelle. The overlap areas were normalized using Python's sklearn. Individual cells were then clustered, and the dataset was downsized by excluding the clusters of the most extreme values. The mean area of overlap was calculated for each MT5-MMP variant and

normalized to pcDNA. Finally, outliers were detected with the Tukey method and the values were used to visualize the results and perform Bayesian statistics.

After averaging the values by plasmid and organelle, the PCA function from sklearn was used with two principal components (n components=2). For cluster analysis, the function clustermap from the seaborn package was used.

A complete list of Python and package versions is provided at: github.com/RiveraLabINP/BelioMairal_2024.

ELISA

An ELISA kit (KHB3481, ThermoFisher Scientific) was used to measure secreted Aβ40 in cell supernatants, which were collected and stored at -80°C until analysis. Samples were diluted to match the detection range and the manufacturer's protocol was followed throughout the procedure. The pcDNA condition values were used to normalize all other values.

Proximity ligation assay

Colocalization between C99 and MT5-MMP constructs was performed by proximity ligation assay (PLA) using the DuoLink© In Situ system. All volumes were adjusted to perform the procedures in 96-well plates. Unconjugated goat anti-rat (112-005-003, Jackson ImmunoResearch) and goat anti-rabbit (111-005-003, Jackson ImmunoResearch) antibodies were conjugated with DuoLink© PLA orange probes (DUO96030-1KT, Sigma-Aldrich) following the manufacturer's instructions and stored at 4°C. Cells were stained using the immunofluorescence protocol as described above. Secondary antibody binding and further procedures were performed according to DuoLink© In situ orange detection kit (DUO92007-100RXN, Sigma-Aldrich). Cell nuclei were stained with Hoechst 33342 as described above.

Peptide synthesis and conjugations

Fmoc–amino acids were obtained from Iris Biotech (Marktredwitz, Germany). All other amino acids and reagents were purchased from Sigma-Aldrich (Saint-Quentin-Fallavier,

France) or Analytical Lab (Castelnau-le-Lez, France). Peptide assembly was performed using a Liberty (CEM®) microwave synthesizer by solid phase peptide synthesis (SPPS) based on the Fmoc strategy. Fmoc–Gly-Wang resin (loading 0.66 mmol/g) were purchased from Iris Biotech and were used as solid support.

Purification and analysis of peptide-based products

Monitoring of reactions and quality controls of the peptide-based intermediates were carried out by liquid chromatography/mass spectrometry (LC/MS) using a Thermo Fisher Scientific UltiMate®3000 system (Waltham, MA, USA) equipped with an ion trap (LCQ Fleet) and an electrospray ionization source (positive ion mode). The LC flow rate was set to 2 mL/min using H2O 0.1%TFA (buffer A) and MeCN 0.1%TFA (buffer B) as eluents. The gradient elution was 10%–90% B in 10 min (quality control) equipped with a C18 Kinetex™ (2.6 µm, 50 mm × 4.6 mm). The heated electrospray ionization source had a capillary temperature of 350 °C. Crude peptides were purified using reverse-phase (RP)-High Pressure Liquid Chromatography (HPLC) on a Thermo Fisher Scientific UltiMate®3000 system equipped with a C18 Luna™ (5 µm, 100 mm × 21.2 mm). The detection was performed at 214 nm. The elution system comprised H2O 0.1%TFA (buffer A) and MeCN 0.1%TFA (buffer B). Flow rate was 20 mL/min.

Preparation of p17 and p20

Peptide p17: H-QFAAAAAPQPVTYYKRPVQEWV-COOH and peptide p20: H-QFKNKTGPQPVTYYKRAAAEWV-COOH were synthesized using 0.1 mmol SPPS Fmoc–Gly-Wang resin under microwave activation. Resin was swollen in DMF for 10 min. Deprotection of the fmoc-protecting group was performed using a solution of 20% piperidine in DMF for 200 s under microwave activation at 75 °C. Stepwise assembly of the Fmoc–protected-amino-acids were performed under microwave activation using standard Fmoc peptide chemistry. Double coupling times of 240 s were used with a solution of Fmoc–amino acid (1 eq), Oxyma (10 eq excess; 1 M) in DMF, and DIC (5 eq excess; 1 M) in DMF under microwave activation at 90 °C. Double coupling was used for R amino acids to improve yield. Finally, the peptidyl-resin was washed 3 times with DCM and then treated with TFA/TIS/H2O

(95:2.5:2.5) containing DTT (10 mg/1mL) at RT for 4 h. The cleavage solution was recovered, concentrated under N2 flow, precipitated with cold diethyl ether and washed 2 times with cold diethyl ether. The crude products were dissolved in an H2O + 0.1%TFA /MeCN + 0.1% TFA (1:1) mixture and lyophilized. The crude peptide was purified using preparative RP-HPLC as described previously to obtain p17 and p20 as white powders (p17: 60 mg, 24%; p20: 52 mg, 20%).

Production of variable heavy domain of heavy chain (VHH) C5

Phagemid encoding VHH C5 nanobody was transformed in the E. coli BL21DE3 strain. Transformed bacteria were grown in 200 ml of 2YTA until 0.5 < OD600 < 0.8 and induced with 100 µM IPTG overnight at 30 °C with shaking (250 rpm). Bacteria were pelleted and lysed by freeze-thawing and BugBuster® Protein Extraction Reagent (Novagen, Pretoria, South Africa). After a centrifugation step (3000 g, 20 min), VHH C5 was purified from the supernatant using metal affinity chromatography, TALON® Superflow™ (GE Healthcare), according to the manufacturer's instructions. Bound molecules were eluted with 250 mM imidazole, which was eliminated using PD-10 Desalting column (GE Healthcare). An additional gel filtration step using a Superdex 75 column (Cytiva, Marlborough, USA) was performed to remove endotoxins. The purified VHH was validated for its quality and purity by LC-MS on a Orbitrap Exploris apparatus (Thermo Fisher Scientific).

Chemical conjugation of VHH C5 and p17

First, C5-PEG2-BCN was prepared. An Eppendorf vial was filled with VHH C5 (8.0 mg, 539 nmol, 2.0 mL in PBS 1X), BCN-PEG2-NH2 (5.2 mg, 16170 nmol, 0.5 mL in PBS 1X) and BTG (10.8 U, 0.08 mL). The reaction mixture was left overnight at RT and purified by size exclusion chromatography hiload 16/600 Superdex 75 pg using PBS 1X as an eluent to give C5-PEG2-BCN as a colorless solution (6.8 mg, 79%, 2.1 mL in PBS 1X). Finally, in an Eppendorf vial were introduced respectively C5-PEG2-BCN (1.8 mg, 119 nmol, 557 µL in PBS 1X) and p17 (1.0 mg, 356 nmol, 234 µL in PBS 1X). The reaction mixture was left overnight at RT and purified by size exclusion chromatography Superdex 10/300 increase 75

GL using PBS 1X as eluent to give C5-p17 as a colorless solution (1.5 mg, 72%, 290 µL in PBS 1X).

Statistics

Frequentist statistics were performed using GraphPad Prism 10.2.3 for MacOSX (GraphPad Software). Unless otherwise stated, all tests were ANOVA with Dunnett's post hoc multiple comparison test, comparing against the control condition of each experimental set. The same software was used to generate the graphs, where the p-values are represented with * p value < 0.05, ** p value < 0.01, *** p value < 0.001, and **** p value < 0.0001.

For Bayesian statistics, JASP 0.18.3 (JASP team) was used to perform Bayesian ANOVA with post hoc tests. Prior odds were the software default values, and the Bayes factor was calculated comparing the alternative (1) against the null (0) model (BF10). The software directly provided the logarithmic BF10 (LogBF10).

All statistical analyses were performed with at least three independent experiments.

RESULTS

Modulation of C99 and Aβ levels by different MT5-MMP variants

We previously showed that deletion of the intracytoplasmic (IC) domain of MT5-MMP alone or together with the transmembrane (TM) domain, respectively termed EXT/TM and EXT, significantly reduced C99 levels when either construct was expressed in HEK cells with a plasmid encoding C99. In contrast, depleting the extracellular domains (EXT) of MT5-MMP, hereafter referred to as TM/IC, was sufficient to reproduce the pro-amyloidogenic effects of MT5-MMP in cells overexpressing C99[4]. To better understand the role of certain domains or sequences in controlling C99 and Aβ levels, we generated various plasmids encoding mutant forms of MT5-MMP (see Fig. 1A for a schematic of the constructs) that were cotransfected with C99 in HEK cells. None of these cotransfections affected cell survival as measured by the MTT test (Fig. 1B).

It was unclear from our previous work whether proteolytic activity of EXT could account for its anti-amyloidogenic effects. Accordingly, we generated an inactive EXT construct by replacing the Glu283 residue of the catalytic site with alanine (hereafter referred to as ΔEXT). Coexpression of EXT, EXT/TM, and ΔEXT in HEK cells induced a decrease in C99 levels by 83%, 71%, and 74%, respectively, compared to the MT5-MMP TM/IC control, as revealed by western blot (Fig. 1C). This indicates that the catalytic activities of EXT and EXT/TM are not responsible for C99 decrease in the absence of the TM and IC domains. Under these conditions, we also observed a significant decrease in Aβ levels in the supernatant of cells expressing EXT, as assessed by ELISA, whereas ΔEXT cells exhibited Aβ levels close to control (Fig. 1D). This suggests that inactivation of the catalytic domain may direct some of C99 toward Aβ production, as opposed to EXT.

Next, we also sought to determine whether changes in C99 were primarily due to the exclusion of the TM or IC domain, or both. To this end, we generated whole-domain substitutions to identify selective modifications of the MT5-MMP TM or IC amino acid sequences potentially sufficient to cause a significant reduction in C99 levels. These substitutions were based on previously reported functional differences between MT5-MMP and its close homologue MT1-MMP, in which suppression of its IC domain caused a strong increase in C99 levels, in contrast to the decrease caused by suppression of the MT5-MMP IC

domain[4], herein confirmed. To assess the influence of sequence divergence between the two proteinases, we generated one construct encoding the TM of MT5-MMP and the IC of MT1-MMP (namely TM5/IC1) and another with the reverse composition (TM1/IC5) (see Fig. 1A). TM5/IC1 expression maintained C99 levels while reducing Aβ secretion by 67% (Fig. 1E, F). In contrast TM1/IC5 significantly decreased C99 levels by 69% but maintained Aβ levels compared to TM/IC control (Fig. 1E, F). Overall, the contrasting results for C99 and Aβ with both chimeras indicate a distinct influence on C99 processing, depending on the presence of MT5-MMP TM or IC domains.

MT5-MMP non-catalytic variants control C99 processing

We next investigated the fate of C99 by modulating enzymatic systems potentially involved in C99 degradation. These include the proteasome, inhibited by lactacystin (LACT), γ-secretase, inhibited by ELND006 (D6), the autophagolysosome system, inhibited by Bafilomycin A1 (BAFA1), and cathepsin B, inhibited by CA-074-Me (CA074), which has no effect on canonical APP secretases[16].

In EXT-expressing cells, we found that only LACT treatment caused a significant recovery of C99 levels, whereas all the other inhibitors had no effect (Fig. 1G), indicating a prominent role of proteasome in C99 degradation upon coexpression with EXT. Similarly, in the ΔEXT group, treatment with LACT also induced a significant recovery of C99, whereas D6 and CA074 had no effect (Fig. 1H). Considering that coexpression of ΔEXT and C99 maintains Aβ levels, failure of D6 to recover C99, suggests that EXT catalytic activity hinders Aβ generation. BAFA1 treatment induced a significant 331% recovery of C99 levels in ΔEXT-cotransfected cells, suggesting that the inactivation of the MT5-MMP catalytic domain, partially redirects C99 to lysosomal compartments. These data indicate that the proteasome is the primary processing machinery of C99 in the presence of EXT or ΔEXT, with an alternative degradation pathway involving EXT catalytic activity in lysosomal compartments. CA074 failed to recover C99 levels in EXT- or ΔEXT-expressing cells (Fig. 1G, H), suggesting that the inhibition of this lysosomal enzyme is insufficient to restore C99 levels and block Aβ production.

The prominent role of the proteosome in C99 processing in the presence of MT5-MMP TM and IC prompted us to focus on its modulation and compare it with γ-secretase, the main processing pathway to convert C99 in Aβ. Analyses of these two pathways in the presence of each chimera gave completely different results. LACT and D6 had no effect on C99 levels in the presence of TM5/IC1 (Fig. 1I). In contrast, LACT and D6 increased C99 levels by 212% and 323%, respectively, in cells expressing the TM1/IC5 variant (Fig. 1J), suggesting that both the proteasome and γ-secretase mediate the reduction in C99 levels mediated by this chimera.

A specific cluster of amino acid deletions in the IC domain induces a reduction in C99 and Aβ levels

We next investigated whether the deletion of small clusters of IC residues from MT5-MMP could mimic the decrease in C99 levels caused by deletion of the entire IC domain. As mentioned above, the amino acid deletions were chosen based on the differences with the IC domain of MT1-MMP that may be involved in the opposite effects observed after deletion of the IC domain of MT5-MMP and MT1-MMP[4]. From the N-terminus to the C-terminus, the deletions were as follows: KNKTG, QPVT, YK, PVQ, and EWV (Fig. 2A). None of the mutant variants affected cell survival in HEK cells coexpressing C99 (Fig. 2B). On average, the deletions tended to reduce C99 levels by 40% ± 10%, but only the 53% reduction exhibited by the KNKTG deletion reached statistical significance (Fig. 2C).

Sequence substitutions in the IC domain modulate C99 and Aβ levels

The limited changes in C99 levels after targeted deletions could imply conformation alterations in the structure of the IC domain that interfere with the physiological effects of MT5-MMP variants. To prevent this, we instead introduced alanine (ala) substitutions in the same clusters and added a construct where all selected amino acids were simultaneously replaced with ala (All). No effects on cell survival were observed under these conditions (Fig. 2B). When coexpressed with C99 in HEK cells, only the mutant variants (ala)KNKTG or (ala)PVQ significantly reduced C99 levels (69% and 51%, respectively) compared with the TM/IC control, as shown by western blot using the anti-CTF antibody (Fig. 2D). Likewise, the

All variant caused a significant 69% reduction in C99 (Fig. 2D). In contrast, ala substitutions in the PDZ-binding EWV motif preserved C99 levels equivalent to those of TM/IC (Fig. 2D).

Among all the MT5-MMP with the potential to regulate C99 levels, only the KNKTG substitution significantly decreased (72%) Aβ levels (Fig. 2E), suggesting its prominent role in halting C99 and Aβ accumulation. In contrast, the (ala)EWV preserved comparably high levels of both C99 and Aβ to the TM/IC control.

Decreased C99 levels after (ala)KNKTG expression could result from changes in the proteolytic degradation of C99. Therefore, we treated HEK cells with LACT and D6 after co-transfection with C99 and either TM/IC, TM/IC(ala)KNKTG, or TM/IC(ala)EWV. LACT and D6 significantly restored C99 levels when co-transfected with TM/IC (Fig. 2F). In contrast, C99 levels in the TM/IC(ala)KNKTG group remained unchanged upon treatment with LACT or D6 (Fig. 2G), suggesting an alternative degradation pathway to the proteasome or γ-secretase. In HEK cells cotransfected with TM/IC(ala)EWV, only D6 increased C99 levels (Fig. 2I), indicating that ala substitution in the EWV motif favor processing of C99 by γ-secretase rather than the proteasome. These significant changes in C99 fate associated with MT5-MMP variants may reflect translocation of these variants to subcellular compartments that facilitate C99 processing by specific proteolytic systems.

MT5-MMP variants alter the pattern of subcellular localization of C99

To determine the influence of MT5-MMP variants on the subcellular distribution of C99, and thus the potential impact on its metabolism, we co-transfected human retinal pigment epithelial cells (RPE1) with HA N-terminally tagged C99 (HA-C99) and MT5-MMP variants known to differentially modulate C99 processing (Fig. 3A). RPE1 are highly adherent and of an optimal size to analyze subcellular protein distribution with high-throughput confocal microscopy. In addition, these cells do not express detectable levels of MT5-MMP (Fig. 3B) and, like neural cells, are of embryonic neuroectodermal origin[17]. We used anti-HA antibodies to detect HA-C99 and combined them with antibodies targeting cell organelles from the endomembrane system (early endosomes, Golgi apparatus, endoplasmic reticulum (ER), and lysosomes) to study the subcellular localization of HA-C99 using immunofluorescence. We

acquired and analyzed the images using quantitative unbiased HCS. We used pcDNA as a reference to calculate HA distribution changes as a ratio of MT5-MMP variants to pcDNA.

The distribution of the HA signal changed under the influence of different MT5-MMP variants (Fig. 3C). Notably, all MT5-MMP variants caused an overall reduction in HA signal within the Golgi apparatus (27%±12) and the ER (14%±6) relative to the pcDNA control. In contrast, we observed inconsistent changes in HA signal among MT5-MMP variants in early endosomes (10%±10), accompanied by a slight increase (11%±9) in the lysosomal HA signal (Fig. 3C). However, absolute quantification is insufficient to assess the complexity of HA signal distribution in different organelles under the influence of different MT5-MMP variants. Accordingly, we conducted a principal component analysis (PCA) using two principal components, which collectively account for 75% of HA signal variability, to visualize our data structure summarizing the effects of the MT5-MMP variants on C99 distribution (Fig. 3D). Both pcDNA and TM/IC(ala)EWV were isolated from the main cluster of MT5-MMP variants, indicating that coexpression of either of these two constructs leads to unique HA-C99 distribution patterns. In addition, three distinct groups emerged within the main cluster: those with MT5-MMP TM (EXT/TM, TM/IC, TM/IC(ala)KNKTG), those without MT5-MMP TM (EXT, TM1/IC5), and the TM5/IC1 chimera positioned between these groups. These results suggest: i) that HA-C99 distribution in different organelles varies depending on the coexpression of MT5-MMP variants, and ii) that the presence of MT5-MMP TM determines the subcellular localization of HA-C99.

To assess the effect of MT5-MMP constructs on HA-C99 distribution in each organelle, we performed a cluster analysis with the results of Bayesian ANOVA followed by multiple comparison tests. The natural logarithm of Bayes Factor 10 (LogBF10) quantifies the likelihood of differences in means between groups, providing a measure of the posterior probability of the alternative over the null hypothesis[18]. For example, a LogBF10 value of -1.1 infers that the null hypothesis is three times more likely, 0 indicates equal probability for both, and 1 implies the alternative hypothesis is about three times more probable. Without the restrictions of conventional frequentist methods that rely on p-values, the Bayesian analysis provides a more quantitative criterion for evaluating group differences. In the context of our results, LogBF10 provides a quantitative framework for interpreting whether variations in the

absolute quantification of HA signal are sufficient to support a difference in means or if the evidence remains inconclusive (due to high variability, small number of replicates, etc.).

We calculated the sum of LogBF10 values for each comparison of the effect of individual MT5-MMP variants on HA-C99 signal in each organelle to create a cluster map that visually represents the strength of evidence for variability in different constructs across multiple organelles (Fig. 3E, F). TM/IC(ala)EWV differed from other constructs in HA signal distribution within the Golgi (16.83), ER (2.15), and lysosomes (3.63). However, other MT5-MMP variants altered HA-C99 distribution in one or another specific cellular compartment: TM1/IC5 in the ER (4.57), EXT/TM in the endosomes (4.30), and EXT in the Golgi (1.60) (Fig. 3E, F).

MT5-MMP variants heterogeneously determine HA-C99 subcellular localization

Bayesian analysis indicated that all MT5-MMP constructs altered the subcellular distribution of HA-C99 to some extent compared to the pcDNA control, but certain MT5-MMP variants distinctly stood out. Therefore, we delved deeper into the individual differences in HA signal in each organelle for each MT5-MMP construct by analyzing the LogBF10 values for each individual comparison in the post-hoc analysis (Fig. 4A-E).

Co-staining of EEA1 and HA (HA-C99) showed subtle changes in HA-C99 levels in early endosomes. Only EXT/TM increased (+13%) HA-C99 translocation into early endosomes compared to pcDNA (LogBF10 = 2.21), TM/IC (LogBF10 = 1.05), and TM5/IC1 (LogBF10 = 1.58) (Fig. 3F, 4D). This suggests that MT5-MMP EXT and/or TM, but not MT5-MMP IC, favors the presence of HA-C99 in $EEA1^{+}$ vesicles.

We then examined the Golgi apparatus, which is involved in protein packaging and compartmentalization. All MT5-MMP variants induced a significant reduction (between 15% and 45%) in HA-C99 compared with pcDNA (Fig. 3F, 4C). Among them, TM/IC(ala)EWV showed the strongest effect, with a significant reduction of 45% and a LogBF10 of 12.89. In addition, HA-C99 reduction in the Golgi was more pronounced in TM/IC(ala)EWV (-45%) than in EXT (-16%) (LogBF10 = 2.21), EXT/TM (-17%) (LogBF10 = 0.97), and TM1/IC5 (-15%) (LogBF10 = 1.78). This suggests that the presence of MT5-MMP TM associated with an IC structure facilitates the translocation of HA-C99 outside the Golgi apparatus.

We next wondered whether the effects of MT5-MMP variants might occur upstream of the Golgi, in the ER, which is the endomembrane organelle where most protein synthesis takes place. All MT5-MMP variants differentially reduced HA-C99 levels in the ER compared with pcDNA (Fig. 3F, 4B). In particular, TM1/IC5 reduced HA-C99 levels in the ER by 17% compared to pcDNA (LogBF10 = 4.68), which is a greater reduction than TM/IC(ala)EWV (-4%) (LogBF10 = 2.05). The different levels of HA signal in the ER suggest that the presence of MT5-MMP variants induces the exit of HA-C99 to other cellular compartments, some variants being more effective than others.

Based on our previous results, the levels of co-localization between early endosomes and HA-C99 indicate that EXT/TM preferentially transports HA-C99 from the ER/Golgi to early endosomes, whereas other MT5-MMP variants may translocate HA-C99 into other cellular compartments. The dynamics of HA-C99 distribution in lysosomes were similar under different conditions. The two constructs carrying mutations in the intracellular domain, TM/IC(ala)KNKTG and TM/IC(ala)EWV, differed mainly from pcDNA (Fig. 3F, 4E), with an increase in HA-C99 colocalization with lysosomes of 18% (LogBF10 = 0.97) and 21% (LogBF10 = 5.27), respectively. Although TM/IC had low LogBF10 values compared to pcDNA (LogBF10 = 0.13), it increased HA-C99 in lysosomes by 18%, which is similar to TM/IC(ala)KNKTG and TM/IC(ala)EWV (18% and 21%, respectively), whose LogBF10 values are consistent. Thus, the presence of MT5-MMP TM and IC (intact or mutated) increases the presence of HA-C99 in lysosomes.

Overall, MT5-MMP variants that preserve high levels of C99 and secreted Aβ (i.e., TM/IC and TM/IC(ala)EWV), were more efficient at reducing HA levels in the Golgi while maintaining higher levels in the ER compared to variants that reduce both C99 and Aβ (i.e., EXT and TM/IC(ala)KNKTG). Furthermore, MT5-MMP TM and IC appear to play an important role in the subcellular sorting of HA-C99, promoting the exit of HA-C99 from the Golgi and its translocation into lysosomes.

MT5-MMP modifications alter colocalization with HA-C99

Based on the previous data, MT5-MMP variants (Fig. 5A) are likely to alter the fate of C99 by affecting its distribution within the endomembrane system. However, whether these

changes are driven by proximal interactions between MT5-MMP variants and C99 remains unclear. To address this issue, we performed a proximity ligation assay (PLA) using our RPE1 cell-based model[19]. PLA detects when two target proteins are within less than 40 nm apart. Here, HA-C99 and MT5-MMP were targeted using antibodies against the HA and Flag tags present in their N-terminus, respectively. For quantitative analysis, we used pcDNA as a reference control and subtracted the number of positive spots detected in pcDNA from those observed in the MT5-MMP variants. This adjustment was made by considering the number of positive spots in pcDNA as the baseline for nonspecific binding.

Quantification of HA-C99 colocalization differed between all MT5-MMP variants compared to pcDNA. Individually, TM/IC and TM1/IC5 cells had the highest number (25 spots each) of PLA+ spots per cell (Fig. 5B, C). Despite absolute differences, TM/IC variability projects low LogBF10 numbers in individual comparisons with other constructs (Fig. 5D). TM1/IC5 (25 spots) showed increased colocalization with HA-C99 compared to the TM5/IC1 chimera (10 spots) (LogBF10 = 1.56) and EXT (13 spots) (LogBF10 = 1.41). TM/IC(ala)EWV (21 spots) was the third construct with a high number of PLA^+ spots, exceeding the 13 spots of EXT (LogBF10 = 0.51) and the 10 of TM5/ICI (LogBF10 = 0.91). Finally, compared with EXT/TM (18 spots), TM5/IC1 (10 spots) showed reduced colocalization with HA-C99 (LogBF10 = 1.17) (Fig. 5 A-C). Taken together, our results indicate that the MT5-MMP IC domain plays a role in mediating the colocalization (and eventually the interaction) of the proteinase with HA-C99. However, KNKTG or EWV substitutions were insufficient to significantly decrease the proximal interactions of MT5-MMP with C99, suggesting that these IC mutants retain the ability to interact with C99, while at the same time driving it to other subcellular compartments.

MT5-MMP-based peptides promote C99 degradation

The ability of (ala)KNKTG to reduce C99 and Aβ levels, coupled with its capacity to colocalize with C99, suggests its potential as a framework for designing mimetic peptides that prevent C99 accumulation. We sought to further test this hypothesis by using MT5-MMP IC peptidomimetics containing mutations that reduced C99 levels when overexpressed by plasmid transfection. We synthesized two peptides, hereafter referred to as p17 (KNKTG substitution)

and p20 (PVQ substitution). The peptides were co-transfected with HA-C99 in HEK cells and left for 48 h, with no cytotoxic effect detected by MTT assay (Fig. 6A, B). Treatment with p20 resulted in a significant decrease of HA-C99 levels by 38% only at the highest concentration of 1000 nM (Fig. 6C). In contrast, p17 induced a dose-response decrease at log scale concentrations of 1, 10, 100 and 1000 nM, reducing HA-C99 by 29%, 35%, 53%, and 41%, respectively, which was statistically significant for the latter three concentrations (Fig. 6D). Given its higher efficacy in reducing C99 levels, we developed a strategy to deliver p17 intracellularly without relying on transfection agents. To this end, we conjugated p17 to C5 (C5p17), a VHH (nanobody) that binds to the transmembrane transferrin receptor (TfR), enabling endocytosis and internalization[20]. We confirmed that the addition of C5 preserves the properties of p17 (Fig. 6D) Figure 3C, as the transfection of C5p17 maintained the reduction of HA-C99 levels by 37%, 37% and 36% in HEK cells at 1nM, 10 nM and 100 nM, respectively (Fig. 6E).

After western blot confirmation of TfR expression in HEK cells (Fig. 6F), we conducted free uptake experiments of C5p17 (without transfecting agent) 24 h after expression of HA-C99. We confirmed that the free uptake of C5p17 had no cytotoxic effects on HEK cells (Fig. 6G), while it significantly reduced C99 levels by 69% at the 10 nM concentration (Fig. 6H).

Our results demonstrate the importance of non-catalytic C-terminal domains of MT5-MMP in regulating C99 and Aβ accumulation, in concert with different protein processing pathways. We also highlight the relevance of exploiting the amino acid sequence of the C-terminal domain of MT5-MMP to generate molecular tools that help prevent the accumulation of C99 and Aβ. With the aim of turning our findings into exploitable strategies, we provide pilot results supporting the use of peptidomimetics based on the molecular properties of the IC domain of MT5-MMP, paving the way for the design of functional peptides with therapeutic potential in the context of AD pathogenesis.

DISCUSSION

In recent years, we have identified the pathological contribution of MT5-MMP in cellular and animal models of AD[8,9,21], and also highlighted the importance of its non-catalytic TM and IC domains in controlling C99 and Aβ accumulation[4]. In this study, we identified key mutations in MT5-MMP TM and IC domains that affect functional interactions with C99 and modify its processing and intracellular distribution. Chimeric combinations of MT5-MMP and MT1-MMP TMs and ICs revealed differences of each MT5-MMP domain's proximity interactions with C99 and its subcellular distribution, resulting in different outcomes for C99 and Aβ levels. In addition, individual KNKTG or PVQ ala substitutions in the IC domain reduced C99 levels, but only KNKTG substitutions concordantly reduced Aβ accumulation. Based on these results, we generated and vectorized a synthetic peptide of MT5-MMP IC carrying the KNKTG mutations, which reduced C99 levels and thus reproduced the effect of transfecting plasmids containing this MT5-MMP variant. Overall, the present study identifies specific sets of amino acids in the TM and IC domains that regulate MT5-MMP modulation of C99 fate and demonstrate the viability of these modifications to exploit the properties of MT5-MMP IC for the design of anti-C99 agents.

Modifications in MT5-MMP domains alter C99 fate

As previously shown, MT5-MMP TM/IC in HEK cells overexpressing C99 had comparable effects on C99 and Aβ accumulation to full-length MT5-MMP. In contrast, MT5-MMP lacking the TM/IC or IC domains reduced in C99 and Aβ levels, highlighting the role of the C-terminal domains of MT5-MMP in regulating C99/Aβ metabolism[4]. The catalytic inactivation of MT5-MMP EXT (ΔEXT) did not prevent the decrease in C99 levels (mainly due to proteasome activity), but restored Aβ levels. This suggests that MT5-MMP proteolytic activity was not involved in degrading C99; however it may influence Aβ metabolism, as reported for its close homologue MT1-MMP[4,22,23].

MT1-MMP and MT5-MMP share 60% overall homology, yet only about 20% in their TM and IC domains[24]. This difference may explain the contrasting effects of MT5-MMP and MT1-MMP variants lacking the IC domain, which respectively decrease and increase C99 levels in HEK cells[4]. Accordingly, TM and IC chimeras of both MMPs distinctly regulate C99

and Aβ levels. C99 accumulation and reduced Aβ levels in the presence of TM5/IC1 suggest that the TM of MT5-MMP may protect C99. The sustained C99 levels following LACT or D6 treatment further confirm the role of MT5-MMP TM in shielding C99 from the proteasome and γ-secretase. In contrast, the recovery of C99 levels by LACT and D6 in TM1/IC5-expressing cells indicates that the IC of MT5-MMP facilitates C99 processing. These findings reveal the different influence of the TM and IC domains of MT5-MMP on C99 accumulation and Aβ production, which together may contribute to the role of MT5-MMP in amyloidogenesis.

Mutations of specific amino acids of the MT5-MMP IC prevent C99 and Aβ accumulation

We deleted or substituted several amino acid groups in the MT5-MMP IC domain based on the sequence divergence between MT5-MMP and MT1-MMP. Deletions had negligible effects, except for KNKTG, which significantly decreased C99 levels. This feature was replicated and enhanced by ala substitutions of KNKTG or PVQ. Notably, only KNKTG substitutions also reduced Aβ levels, suggesting a key role for amino acids adjacent to the TM in regulating C99 and Aβ. The inability of LACT and D6 to restore C99 levels in HEK cells expressing TM/IC(ala)KNKTG implies the presence of alternative C99 degradation pathways independent of the proteasome or γ-secretase. This contrasts with previous reports, where overexpressed C99 was mainly processed by the proteasome[4,25]. This emphasizes the importance of TM/IC(ala)KNKTG substitution in regulating C99 metabolism.

Modifications in MT5-MMP IC also induce a pro-amyloidogenic outcome, as ala substitutions in the C-terminal PDZ-binding EWV motif not only maintained C99 and Aβ levels comparable to those in TM/IC, but also enhanced γ-secretase-dependent C99 processing, as demonstrated by the increase in C99 levels only upon D6 treatment. Meanwhile, both LACT and D6 rescued C99 levels in the TM/IC control group. Modifying the C-terminal PDZ-binding motif affects MT5-MMP interactions with Mint3, interfering with MT5-MMP subcellular trafficking[26]. It is noteworthy that Mint3 also binds to APP C-terminal domain and regulates its intracellular traffic[27,28]. In our case, EWV substitution reduced C99 localization in the Golgi by 45%, which could be linked to the disruption of MT5-MMP subcellular localization. This

could increase the export of C99 towards other acidic subcellular compartments where γ-secretase is more active[29–31] and converts C99 to Aβ.

Collectively, these results demonstrate that subtle modifications in the IC domain of MT5-MMP redirect C99 into distinct proteolytic pathways, presumably via changes in C99 subcellular distribution. This highlights the remarkable plasticity of the MT5-MMP IC sequence to modulate C99 and reinforces its potential as a framework for developing anti-C99/Aβ strategies.

MT5-MMP variants alter the patterns of subcellular localization of C99

Our results point to potential changes in the subcellular distribution of C99, which may reveal differences in C99 processing pathways under the influence of specific MT5-MMP variants. This is consistent with the proposed influence of canonical secretases in regulating the subcellular localization of C99/APP and Aβ production[32–34].

PCA revealed differential effects of MT5-MMP variants on HA-C99 distribution, highlighting the importance of the TM domain and the EWV C-terminal amino acids. Cluster analysis of the sum of LogBF10 values confirmed that TM/IC(ala)EWV most strongly influences HA-C99 distribution along the endomembrane system, whereas other MT5-MMP variants limit their effects to single organelles or none at all. This underlines the importance of the MT5-MMP EWV motif in regulating the subcellular localization of C99, likely by preventing C99 interaction with Mint proteins and facilitating γ-secretase cleavage. Apart from Mint3, other members of the Mint family interact with APP metabolites through binding domains, and overexpression of Mint1 or its PTB domain decreased Aβ40 secretion by inhibiting γ-secretase cleavage of C99 in HEK cells[35]. It is thus possible that EWV mutations help C99 bypassing Mint1-dependent inhibition of γ-secretase cleavage.

Individual analysis of each variant revealed a general trend towards reduced HA-C99 levels in different organelles. This was the case in the ER, the main site of protein synthesis, consistent with the stimulation of C99 sorting to other compartments. With respect to the Golgi apparatus, TM/IC(ala)EWV resulted in the greatest reduction in C99 levels (-45%) compared to the other variants. As noted above, substitution of EWV, a PDZ-binding motif in MT5-MMP

TM/IC, might prevent its recycling to the plasma membrane[26], facilitating TM/IC(ala)EWV influence on C99 intracellular sorting.

Expression of the TM/IC(ala)KNKTG and TM/IC(ala)EWV variants significantly increase C99 in lysosomes. The fact that these variants had opposite effects on C99 and Aβ levels, the former being a depressant and the latter being a stabilizer, suggests changes in C99 intracellular trafficking before translocation to lysosomes. Recent findings evidenced intracellular lysosome heterogeneity, which supports the idea that C99 can traffic into molecularly distinct lysosomes[36]. In this line, the inhibition of the autophagosome pathway increases C99 levels in LAMP1+ lysosomes in human neuroglioma cells, whereas autophagosome activation has the opposite effect and prevents γ-secretase cleavage of C99[37]. However, late endosomes-lysosomes are also major sites of C99 conversion into Aβ[31]. It is possible that KNKTG and EWV mutations in MT5-MMP IC distribute C99 into distinct cellular compartments, thereby reaching heterogenous lysosomes containing different proteases through different processing pathways. In addition, TM/IC(ala)EWV-mediated increase in C99 within lysosomes could initiate a pathogenic loop whereby elevated levels of C99 disrupt Ca^{2+} homeostasis in late endosomes and lysosomes, further promoting C99 accumulation[38].

We conclude that different MT5-MMP variants affect C99 subcellular distribution. Moreover, chimeric combinations or minimal mutations MT5-MMP IC distinctly redistribute C99 in cellular compartments of the endomembrane system, indicating a key role of the C-terminal domains of MT5-MMP in C99 trafficking.

Mutations in the IC domain of MT5-MMP determine the colocalization with HA-C99

MT5-MMP and C99 coimmunoprecipitate when overexpressed in HEK cells[4], and changes in C99 subcellular distribution may result from altered proximal interactions with MT5-MMP variants. High throughput PLA screening revealed that TM/IC and TM1/IC5—both containing intact MT5-MMP IC—had the highest level of interaction with HA-C99. This, together with the low levels of PLA+ signal in TM5/IC1, suggests that the IC of MT5-MMP facilitates colocalization and interaction of MT5-MMP and C99, consistent with the TM/IC of MT5-MMP being sufficient to coimmunoprecipitate C99 in HEK cells[4]. The strong reduction of PLA+ spots upon expression of EXT further supports the importance of MT5-MMP IC for

the proximal interaction with C99. However, the increase in EXT/TM colocalization with C99 compared to EXT may indicate that MT5-MMP TM also contributes to proximal localization with C99. Together with the decrease in TM5/IC1, these data suggest that the interface between MT5-MMP TM and IC is important, but not exclusive, for preserving proximal interactions between MT5-MMP and C99. Further investigation of the structural properties of MT5-MMP TM and IC could reveal the mechanisms underlying these dynamics.

The KNKTG or EWV substitutions in MT5-MMP IC maintained colocalization with C99, revealing that these modifications alter C99 processing without disrupting TM/IC interactions with C99. Thus, TM/IC(ala)KNKTG could serve as a reference sequence for designing molecular tools that interact with C99 to modify its the subcellular trafficking and degradation, ultimately decreasing C99 and Aβ levels.

Intracellular delivery of a synthetic MT5-MMP IC peptide mimicking the KNKTG mutation reduces C99 accumulation

Synthetic peptides are widely used as relevant therapeutic tools[39], and offer a potential platform for exploiting the anti-C99 properties of modified versions of the IC domain of MT5-MMP. Both in its unconjugated (p17) and conjugated forms (C5p17), the synthetic peptides containing the (ala)KNKTG sequence significantly reduced C99. On the contrary, the peptide carrying the (ala)PVQ (p20) proved to be less efficient. Collectively, these data provide an initial proof of concept demonstrating the feasibility of MT5-MMP IC-based strategies to promote C99 degradation, likely through mechanisms that affect C99 cellular trafficking. In this vein, a recent study showed that editing the YENPTY motif of the C99 sequence, which is essential for its trafficking, resulted in a stable reduction of C99 and Aβ levels in an AD knock-in mouse model[40]. This highlights the importance of targeting APP metabolites with strategies that affect their trafficking and eventual production of toxic biomolecules. Our study adds to this idea by demonstrating the possibility of using MT5-MMP as a benchmark to generate synthetic peptides, a generally safe therapeutic strategy that also has the advantage of avoiding genome modification.

In this study, we highlight the importance of specific amino acid clusters in non-catalytic domains of MT5-MMP to regulate C99 processing. Our findings reveal that changes in MT5-

MMP sequence define its colocalization with C99 and the subcellular trafficking of the latter. These effects have a distinct impact on C99 and Aβ levels, providing insight into the complex molecular mechanisms governing C99 and Aβ metabolism. Moreover, we also provide insights into the translational potential of exploiting the properties of mutated variants of MT5-MMP TM and IC to promote C99 and Aβ clearance in the context of AD.

Declarations

Ethics approval

All the experimental procedures were conducted in agreement with the authorization by the French Ministry of Research to the laboratory (# 7950), as defined in the directive 2009/41/CE of the European Parliament and the European Council of May 6 2009 for the use of genetically modified organisms.

Availability of data and materials

All the data generated or analyzed during this study are included in this published article and are available from the corresponding author upon reasonable request.

All the analysis files in the form of Jupyter Notebook are uploaded and freely accessible at: github.com/RiveraLabINP/BelioMairal_2024

Acknowledgements

We thank F. Chechler and S. Gon for generously providing HEK cells and RPE-1 cells, respectively. We thank H. Kovacic and F. Parat for their technical advice, and R. Pardossi-Piquard, N. Sergeant, and S. Claeysen for their insightful suggestions on the manuscript.

Competing interests

MK was director of the Institute of Neuropathophysiology, UMR7051 academic neuroscience laboratory supported by the CNRS and Aix-Marseille University, but also co-founder, shareholder and scientific counsel of the VECT-HORUS biotechnology company. The other authors declare that they have no competing interests.

Funding

This work was supported by funding from the CNRS and Aix-Marseille Université and by public grants to overseen by Fondation pour la Recherche Médicale (FRM) and Fondation Plan Alzheimer (ALZ201912009627) to SR, Fondation Vaincre Alzheimer to SR (FVA-

FR20067) by the French National Agency for Research (ANR) MT5-AD (MT5-AD, ANR-22-C18-0024-01). PB-M received a doctoral fellowship from the French government under the Programme Investissements d'Avenir, Initiative d'Excellence d'Aix-Marseille Université via A*Midex (AMX-19-IET-004) and ANR (ANR-17-EURE-0029) funding through NeuroSchool/NeuroMarseille. AK received an international mobility grant under the same program. PB-M also received financial support from Fondation Vaincre Alzheimer.

REFERENCES

1. Rivera S, Khrestchatisky M, Kaczmarek L, Rosenberg GA, Jaworski DM. Metzincin proteases and their inhibitors: foes or friends in nervous system physiology? *J Neurosci*. 2010;30(46):15337-15357. doi:10.1523/JNEUROSCI.3467-10.2010

2. Sekine-Aizawa Y, Hama E, Watanabe K, et al. Matrix metalloproteinase (MMP) system in brain: identification and characterization of brain-specific MMP highly expressed in cerebellum: MT5-MMP: a brain-specific MMP in rat. *European J Neurosci*. 2001;13(5):935-948. doi:10.1046/j.0953-816x.2001.01462.x

3. Jaworski DM. Developmental regulation of membrane type-5 matrix metalloproteinase (MT5-MMP) expression in the rat nervous system. *Brain Res*. 2000;860(1-2):174-177.

4. García-González L, Paumier J, Louis L, et al. MT5-MMP controls APP and β-CTF/C99 metabolism through proteolytic-dependent and -independent mechanisms relevant for Alzheimer's disease. *FASEB J*. 2021;35(7). doi:10.1096/fj.202100593R

5. Rivera S, García-González L, Khrestchatisky M, Baranger K. Metalloproteinases and their tissue inhibitors in Alzheimer's disease and other neurodegenerative disorders. *Cell Mol Life Sci*. 2019;76(16):3167-3191. doi:10.1007/s00018-019-03178-2

6. Ahmad M, Takino T, Miyamori H, Yoshizaki T, Furukawa M, Sato H. Cleavage of amyloid-beta precursor protein (APP) by membrane-type matrix metalloproteinases. *J Biochem*. 2006;139(3):517-526. doi:10.1093/jb/mvj054

7. Willem M, Tahirovic S, Busche MA, et al. η-Secretase processing of APP inhibits neuronal activity in the hippocampus. *Nature*. 2015;526(7573):443-447. doi:10.1038/nature14864

8. Baranger K, Marchalant Y, Bonnet AE, et al. MT5-MMP is a new pro-amyloidogenic proteinase that promotes amyloid pathology and cognitive decline in a transgenic mouse model of Alzheimer's disease. *Cell Mol Life Sci*. 2016;73(1):217-236. doi:10.1007/s00018-015-1992-1

9. Baranger K, Bonnet AE, Girard SD, et al. MT5-MMP Promotes Alzheimer's Pathogenesis in the Frontal Cortex of 5xFAD Mice and APP Trafficking in vitro. *Front Mol Neurosci*. 2017;9. doi:10.3389/fnmol.2016.00163

10. Selkoe DJ, Hardy J. The amyloid hypothesis of Alzheimer's disease at 25 years. *EMBO Mol Med*. 2016;8(6):595-608. doi:10.15252/emmm.201606210

11. Lauritzen I, Pardossi-Piquard R, Bauer C, et al. The -Secretase-Derived C-Terminal Fragment of APP, C99, But Not A , Is a Key Contributor to Early Intraneuronal Lesions in Triple-Transgenic Mouse Hippocampus. *J Neurosci*. 2012;32(46):16243-16255. doi:10.1523/JNEUROSCI.2775-12.2012

12. Py NA, Bonnet AE, Bernard A, et al. Differential spatio-temporal regulation of MMPs in the 5xFAD mouse model of Alzheimerâ€™s disease: evidence for a pro-amyloidogenic role of MT1-MMP. *Front Aging Neurosci*. 2014;6. doi:10.3389/fnagi.2014.00247

13. Pulina MV, Hopkins M, Haroutunian V, Greengard P, Bustos V. C99 selectively accumulates in vulnerable neurons in Alzheimer's disease. *Alzheimer's & Dementia*. 2020;16(2):273-282. doi:10.1016/j.jalz.2019.09.002

14. Kwart D, Gregg A, Scheckel C, et al. A Large Panel of Isogenic APP and PSEN1 Mutant Human iPSC Neurons Reveals Shared Endosomal Abnormalities Mediated by APP β-CTFs, Not Aβ. *Neuron*. 2019;104(2):256-270.e5. doi:10.1016/j.neuron.2019.07.010

15. Schindelin J, Arganda-Carreras I, Frise E, et al. Fiji: an open-source platform for biological-image analysis. *Nat Methods*. 2012;9(7):676-682. doi:10.1038/nmeth.2019

16. Asai M, Yagishita S, Iwata N, Saido TC, Ishiura S, Maruyama K. An alternative metabolic pathway of amyloid precursor protein C-terminal fragments via cathepsin B in a human neuroglioma model. *FASEB J*. 2011;25(10):3720-3730. doi:10.1096/fj.11-182154

17. Klimanskaya I. Retinal Pigment Epithelium. In: *Methods in Enzymology*. Vol 418. Embryonic Stem Cells. Academic Press; 2006:169-194. doi:10.1016/S0076-6879(06)18011-8

18. Keysers C, Gazzola V, Wagenmakers EJ. Using Bayes factor hypothesis testing in neuroscience to establish evidence of absence. *Nat Neurosci*. 2020;23(7):788-799. doi:10.1038/s41593-020-0660-4

19. Söderberg O, Gullberg M, Jarvius M, et al. Direct observation of individual endogenous protein complexes in situ by proximity ligation. *Nat Methods*. 2006;3(12):995-1000. doi:10.1038/nmeth947

20. COHEN R, David M, Khrestchatisky M. Transferrin receptor-binding molecules, conjugates thereof and their uses. Published online July 16, 2020. Accessed July 8, 2024. https://patents.google.com/patent/WO2020144233A1/en

21. Pilat D, Paumier JM, García-González L, et al. MT5-MMP promotes neuroinflammation, neuronal excitability and Aβ production in primary neuron/astrocyte cultures from the 5xFAD mouse model of Alzheimer's disease. *J Neuroinflamm*. 2022;19(1):65. doi:10.1186/s12974-022-02407-z

22. García-González L, Pilat D, Baranger K, Rivera S. Emerging Alternative Proteinases in APP Metabolism and Alzheimer's Disease Pathogenesis: A Focus on MT1-MMP and MT5-MMP. *Front Aging Neurosci*. 2019;11:244. doi:10.3389/fnagi.2019.00244

23. Paumier JM, Py NA, García-González L, et al. Proamyloidogenic effects of membrane type 1 matrix metalloproteinase involve MMP-2 and BACE-1 activities, and the modulation of APP trafficking. *FASEB J*. 2019;33(2):2910-2927. doi:10.1096/fj.201801076R

24. Pei D. Identification and Characterization of the Fifth Membrane-type Matrix Metalloproteinase MT5-MMP. *J Biol Chem*. 1999;274(13):8925-8932. doi:10.1074/jbc.274.13.8925

25. Evrard C, Kienlen-Campard P, Coevoet M, et al. Contribution of the Endosomal-Lysosomal and Proteasomal Systems in Amyloid-β Precursor Protein Derived Fragments Processing. *Front Cell Neurosci*. 2018;12:435. doi:10.3389/fncel.2018.00435

26. Wang P, Wang X, Pei D. Mint-3 Regulates the Retrieval of the Internalized Membrane-type Matrix Metalloproteinase, MT5-MMP, to the Plasma Membrane by Binding to Its Carboxyl End Motif EWV. *J Biol Chem*. 2004;279(19):20461-20470. doi:10.1074/jbc.M400264200

27. Caster AH, Kahn RA. Recruitment of the Mint3 Adaptor Is Necessary for Export of the Amyloid Precursor Protein (APP) from the Golgi Complex. *J Biol Chem*. 2013;288(40):28567-28580. doi:10.1074/jbc.M113.481101

28. Ho A, Liu X, Südhof TC. Deletion of Mint proteins decreases amyloid production in transgenic mouse models of Alzheimer's disease. *J Neurosci*. 2008;28(53):14392-14400. doi:10.1523/JNEUROSCI.2481-08.2008

29. Cai T, Hatano A, Kanatsu K, Tomita T. Histidine 131 in presenilin 1 is the pH-sensitive residue that causes the increase in Aβ42 level in acidic pH. *J Biochem*. 2020;167(5):463-471. doi:10.1093/jb/mvz110

30. Kanatsu K, Hori Y, Ebinuma I, Chiu YW, Tomita T. Retrograde transport of γ-secretase from endosomes to the trans-Golgi network regulates Aβ42 production. *J Neurochem*. 2018;147(1):110-123. doi:10.1111/jnc.14477

31. Maesako M, Houser MCQ, Turchyna Y, Wolfe MS, Berezovska O. Presenilin/γ-Secretase Activity Is Located in Acidic Compartments of Live Neurons. *J Neurosci*. 2022;42(1):145-154. doi:10.1523/JNEUROSCI.1698-21.2021

32. Choy RWY, Cheng Z, Schekman R. Amyloid precursor protein (APP) traffics from the cell surface via endosomes for amyloid β (Aβ) production in the trans-Golgi network. *Proc Natl Acad Sci*. 2012;109(30):E2077-E2082. doi:10.1073/pnas.1208635109

33. Roselli S, Satir TM, Camacho R, et al. APP-BACE1 Interaction and Intracellular Localization Regulate Aβ Production in iPSC-Derived Cortical Neurons. *Cell Mol Neurobiol*. 2023;43(7):3653-3668. doi:10.1007/s10571-023-01374-0

34. Wang J, Gleeson PA, Fourriere L. Spatial–Temporal Mapping Reveals the Golgi as the Major Processing Site for the Pathogenic Swedish APP Mutation: Familial APP Mutant Shifts the Major APP Processing Site. *Traffic*. 2024;25(3):e12932. doi:10.1111/tra.12932

35. King GD, Cherian K, Turner RS. X11alpha impairs gamma- but not beta-cleavage of amyloid precursor protein. *J Neurochem*. 2004;88(4):971-982. doi:10.1046/j.1471-4159.2003.02234.x

36. Bond C, Hugelier S, Xing J, Sorokina EM, Lakadamyali M. Heterogeneity of late endosome/lysosomes shown by multiplexed DNA-PAINT imaging. *J Cell Biol*. 2024;224(1):e202403116. doi:10.1083/jcb.202403116

37. González AE, Muñoz VC, Cavieres VA, et al. Autophagosomes cooperate in the degradation of intracellular C-terminal fragments of the amyloid precursor protein via the MVB/lysosomal pathway. *FASEB J*. 2017;31(6):2446-2459. doi:10.1096/fj.201600713R

38. Bretou M, Sannerud R, Escamilla-Ayala A, et al. Accumulation of APP C-terminal fragments causes endolysosomal dysfunction through the dysregulation of late endosome to lysosome-ER contact sites. *Dev Cell*. 2024;59(12):1571-1592.e9. doi:10.1016/j.devcel.2024.03.030

39. Vlieghe P, Lisowski V, Martinez J, Khrestchatisky M. Synthetic therapeutic peptides: science and market. *Drug Discov Today*. 2010;15(1-2):40-56. doi:10.1016/j.drudis.2009.10.009

40. Aulston BD, Gimse K, Bazick HO, et al. Long term rescue of Alzheimer's deficits in vivo by one-time gene-editing of App C-terminus. *bioRxiv*. Published online June 9, 2024:2024.06.08.598099. doi:10.1101/2024.06.08.598099

FIGURE LEGENDS

Figure 1. Whole-domain mutations modulate the accumulation of C99 and the production of Aβ in HEK cells.

(A) Schematic representation of the MT5-MMP variants used. (B) Graph showing no changes in cell survival measured by the MTT assay 48 h after co-transfection of HEK cells with C99 and different MT5-MMP variants. Absorbance values are expressed in arbitrary units (A.U) and normalized to those of samples treated with transfection reagent alone. (C) Representative western blots showing C99 levels detected with an anti-APP-CTF antibody in HEK cells co-transfected with C99 and TM/IC, EXT, EXT/TM, or ΔEXT. The graph shows C99 levels normalized to actin as a protein loading control and the pcDNA condition. (D) Graphical representation of Aβ40 levels in the supernatants of HEK cells co-transfected with C99 and TM/IC, EXT, EXT/TM or ΔEXT. Values were normalized to the pcDNA condition for each experiment. (E) Representative western blots showing C99 levels detected with an anti-APP-CTF antibody in HEK cells co-transfected with C99 TM/IC, EXT, EXT/TM, TM5/IC1 or TM1/IC5. The graph represents C99 levels normalized to actin as a protein loading control and the pcDNA condition. (F) Graphical representation of Aβ40 levels in the supernatants of HEK cells co-transfected with C99 and with TM/IC, EXT, EXT/TM, TM5/IC1 or TM1/IC5. Values were normalized to the pcDNA condition for each experiment. (G-J) Representative western blots showing C99 levels detected with an anti-APP-CTF antibody in HEK cells co-transfected with C99 and (G) EXT, (H) ΔEXT, (I) TM5/IC1 or (J) TM1/IC5 variants. The corresponding actin-normalized quantifications are shown below each immunoblot. Cells were treated for 20 h with inhibitors of C99 processing pathways: proteasome (lactacystin; LACT 10 μM); γ-secretase ELND006 (D6 1 μM); cathepsin (B CA-074 Me; CA074 10 μM); and autophagolysosomal pathway (bafilomycin A1; BAFA 50 nM). DMSO was used as control vehicle. ANOVA followed by Dunnett's post hoc test compared to control condition. Values are expressed as mean ± SEM of at least 3 independent experiments. P-values are shown as * $p < 0.05$, ** $p < 0.01$, *** $p < 0.001$, and **** $p < 0.0001$.

Figure 2. Mutation of specific MT5-MMP IC residues decreases C99 and Aβ levels in HEK cells.

(A) Schematic representation of the MT5-MMP variants used. The amino acid groups in red (KNKTG, QPVT, YK, PVQ, and EWV) were either deleted or substituted by ala. (B) Graph showing no changes in cell survival measured by the MTT assay 48 h after co-transfection of HEK cells with C99 and different MT5-MMP variants. Absorbance values are expressed in arbitrary units (A.U) and normalized to those of samples treated with the transfection reagent alone. (C & D) Representative western blots showing C99 levels detected with an anti-APP-CTF antibody in HEK cells co-transfected with C99 and TM/IC or TM/IC with deletions (C) or ala substitutions (D) in KNKTG, QPVT, YK, PVQ or EWV. In addition, all amino acids were substituted with alanine (All) in D. The graphs below show the levels of C99 normalized to actin as a protein loading control and the pcDNA condition. (E) Graphical representation of Aβ40 levels in the supernatants of HEK cells co-transfected with C99 and TM/IC, TM/IC(ala)KNKTG, TM/IC(ala)PVQ, TM/IC(ala)EWV or TM/IC(ala)All. Values were normalized to the pcDNA condition for each experiment. (F-H) Representative western blots showing C99 levels detected with an anti-APP-CTF antibody in HEK cells co-transfected with C99 and (F) TM/IC, (G) TM/IC(ala)KNKTG or (H) TM/IC(ala)EWV and treated for 20 h with lactacystin (LACT 10 μM) or γ-secretase inhibitor (ELND006; D6 1μM). DMSO was used as a control vehicle. The graphs below represent C99 levels normalized to actin as a protein loading control. ANOVA followed by Dunnett's post hoc test compared to control condition. Values are expressed as mean ± SEM of at least 3 independent experiments. P-values are shown as * $p < 0.05$, ** $p < 0.01$, and *** $p < 0.001$.

Figure 3. Effect of specific MT5-MMP IC domain mutations on the subcellular distribution of C99 in RPE1 cells.

(A) Schematic representation of the MT5-MMP used. The amino acid groups in red (KNKTG and EWV) were substituted by ala. (B) Western blotting showing the lack of MT5-MMP expression in lysates of both HEK and RPE1 cells. (C) Heatmap representing the quantification of the area of HA^+ signal in RPE1 cells overlapping with each organelle as a function of the MT5-MMP variant co-transfected with HA-C99 and relative to pcDNA in percent change. (D)

Principal component analysis (PCA) of the quantification heatmap in C, constructed with two components representing 75% of the total variability of the data. Each MT5-MMP variant clustered with variants that had similar profiles of change relative to pcDNA. (E) Cluster map representing changes in (D) based on Bayesian ANOVA. The values are the summed LogBF10 values of multiple comparisons between MT5-MMP variants in each organelle, representing the statistical strength of variability in HA overlap with organelles for each MT5-MMP variant. The higher the values, the stronger the statistical evidence that a given MT5-MMP variant induces changes in HA overlap relative to all other variants in the same organelle. The lower the values, the weaker the statistical evidence for such changes. Higher values are shown in light to dark red, and lower values are represented in light to dark blue. In this cluster map, TM/IC(ala)EWV particularly affects HA overlap in the Golgi, ER, and lysosomes relative to all other MT5-MMP variants; and TM1/IC5 specifically affects HA signal overlap with the ER. However, compared with the other variants, EXT did not alter the HA overlap with lysosomes compared to the other variants. (F) Representative images of HA signal overlapping with organelle immunolabeling in RPE1 co-transfected with HA-C99 and MT5-MMP variants. The organelles are shown in magenta, and the HA signal is shown in cyan. The multiline plots show the distribution of fluorescence intensity along the 20 µm yellow line in the image, representing the colocalization of fluorescence along the line. Scale bar: 10 µm.

Figure 4. LogBF10 values of individual differences in the subcellular localization of HA-C99 in RPE1 cells transfected with different MT5-MMP variants.

(A) Schematic representation of the MT5-MMP used. Amino acid groups in red (KNKTG and EWV) were replaced by ala. (B-E) Diagonal correlation matrices represent LogBF10 values for each comparison in a Bayesian ANOVA, with post-hoc multiple comparisons of the percentage of change in HA overlap induced by different MT5-MMP variants relative to pcDNA in early endosomes (B), Golgi (C), endoplasmic reticulum (D) and lysosomes (E). Higher levels are shown in light to dark red, and lower values are shown in light to dark blue. For instance, in (C) Golgi, the LogBF10 value from comparing pcDNA to TM/IC(ala)EWV indicates a significant reduction in HA signal in the Golgi. Values close to 0 indicate that there is insufficient evidence to determine whether there is a difference. Negative values represent strong evidence supporting no difference in the comparison of means.

Figure 5. Mutating residues in the MT5-MMP IC domain disrupts interactions with C99.

(A) Schematic representation of the MT5-MMP variants used. The amino acid groups in red (KNKTG and EWV) were replaced by ala. (B) Representative HCS microphotographs showing segmented (nuclear and cytoplasmic borders) RPE1 cells co-transfected with HA-C99 and the MT5-MMP variants described in (A). Orange dots correspond to PLA^+ spots reflecting the proximity of HA (HA-C99) and Flag (MT5-MMP variant) at less than 40 nm, revealed by antibodies conjugated to DuoLink© orange oligos. The scale bar is 10 µm. (C) Quantification of the number of PLA^+ spots in each MT5-MMP variant. PLA^+ spots in pcDNA were subtracted from the other conditions, as we considered them to represent the non-specific background signal. Values representing a high number of PLA^+ spots are purple and darker, while lower PLA^+ spots are represented in lighter purple colors or white. (D) Diagonal correlation matrix representing the LogBF10 values for each comparison in a Bayesian ANOVA with post-hoc multiple comparisons of the number of PLA^+ spots between different MT5-MMP variants. Higher values are represented in light-to-dark red, and lower values are represented in light-to-dark blue. For instance, the difference in PLA^+ spots between TM1/IC5 and TM5/IC1 has a LogBF10 value of 1.56, suggesting that there is a difference in the average number of PLA+ spots per cell between these two variants.

Figure 6. Effects of modified peptides of the MT5-MMP IC domain on C99 levels in heterologous cell lines.

(A-B) Amino acid sequence of peptide p20 (A) and peptide p17 (B), based on the MT5-MMP IC, where PVQ and KNKTG were substituted by ala (in red). The graphs below show the absence of cytotoxicity measured by the MTT assay 48 h after cotransfection with C99 and p20 (A) or p17 (B). Absorbance values are expressed in arbitrary units (A.U.) and normalized to those of samples treated only with transfection reagent alone. (C-E) Representative western blots of HEK cells co-transfected with HA-C99 and p20 (C), p17 (D) or p17conjugated conjugated with a C5 VHH (C5p17) (E) at different concentrations. HA-C99 was detected with a rat anti-HA antibody. The graphs below show semi-quantifications of HA-C99 levels normalized to actin as a protein loading control. (F) Western blots showing TfR

immunodetection in HEK cell lysates. (G) The graph shows the absence of cytotoxicity in HEK cells as measured by the MTT assay 48 h after transfection with HA-C99 and subsequent treatment with C5p17. (H) Sequence representing the VHH C5 conjugated to p17. Below is a representative western blot of HEK cell lysates transfected with HA-C99 and incubated for 48 h with C5p17 at different concentrations. HA-C99 was detected using a rat anti-HA antibody. The graph below represents semi-quantifications of HA-C99 levels normalized to actin as a protein loading control. Values are expressed as mean ± SEM. P-values are represented by * $p < 0.05$ and ** $p < 0.01$. ANOVA followed by Dunnett's post hoc multiple comparison test, with at least three independent experiments.

TABLES

Table 1. List of the inhibitors with concentration of the stock and final solutions, and manufacturer's references.

Inhibitors				
Inhibitor	**[Stock](µM)**	**Dilution**	**Reference**	**Company**
LACT	**50000**	**1:5000**	**BML-PI104-1000**	**Enzo Life Sciences**
D6	**5000**	**1:5000**	**SML2122**	**Sigma-Aldrich**
BAFA1	**250**	**1:5000**	**B1793**	**Sigma-Aldrich**
CA074	**50000**	**1:5000**	**205531**	**Sigma-Aldrich**

Table 2. List of antibodies with target antigens, host species, working dilutions, references, and the application. PLA stands for proximity ligation assay.

Antibodies					
Target	**Host**	**Dilution**	**Reference**	**Company**	**Application**
Primaries					
APP-CTF	**Rabbit**	**1:1000**	**A8717**	**Sigma-Aldrich**	**Western blot**
Actin	**Mouse**	**1:5000**	**A1978**	**Sigma-Aldrich**	**Western blot**
TfR1	**Rabbit**	**1:1000**	**GTX102596**	**GeneTex**	**Western blot**
Nogo-B	**Sheep**	**1:25**	**AF6034**	**Biotechne**	**Immunofluorescence**
GM130	**Mouse**	**1:200**	**610823**	**BD Biosciences**	**Immunofluorescence**
EEA1	**Mouse**	**1:100**	**sc-365652**	**Santa Cruz Biotechnology**	**Immunofluorescence**
LAMP1	**Rabbit**	**1:300**	**ab24170**	**Abcam**	**Immunofluorescence**
HA	**Rat**	**1:100** **1:100**	**11867423001**	**Roche**	**Immunofluorescence** **PLA** **Western blot**
Flag	**Rabbit**	**1:200**	**14793**	**Cell Signaling Technology**	**PLA**
Secondaries					
Rabbit	**Goat**	**1:800**	**111-005-003**	**Jackson ImmunoResearch**	**PLA**
Rat	**Goat**	**1:800**	**112-005-003**	**Jackson ImmunoResearch**	**PLA**
Mouse-647	**Donkey**	**1:800**	**A32787**	**ThermoFisher Scientific**	**Immunofluorescence**
Rabbit-647	**Donkey**	**1:800**	**A32795**	**ThermoFisher Scientific**	**Immunofluorescence**
Sheep-647	**Donkey**	**1:800**	**A21448**	**ThermoFisher Scientific**	**Immunofluorescence**
Rat-488	**Donkey**	**1:800**	**A48269**	**ThermoFisher Scientific**	**Immunofluorescence**
Rabbit-488	**Donkey**	**1:800**	**A-21206**	**ThermoFisher Scientific**	**Immunofluorescence**
Mouse-594	**Donkey**	**1:800**	**A-21203**	**ThermoFisher Scientific**	**Immunofluorescence**

FIGURES

Figure 1

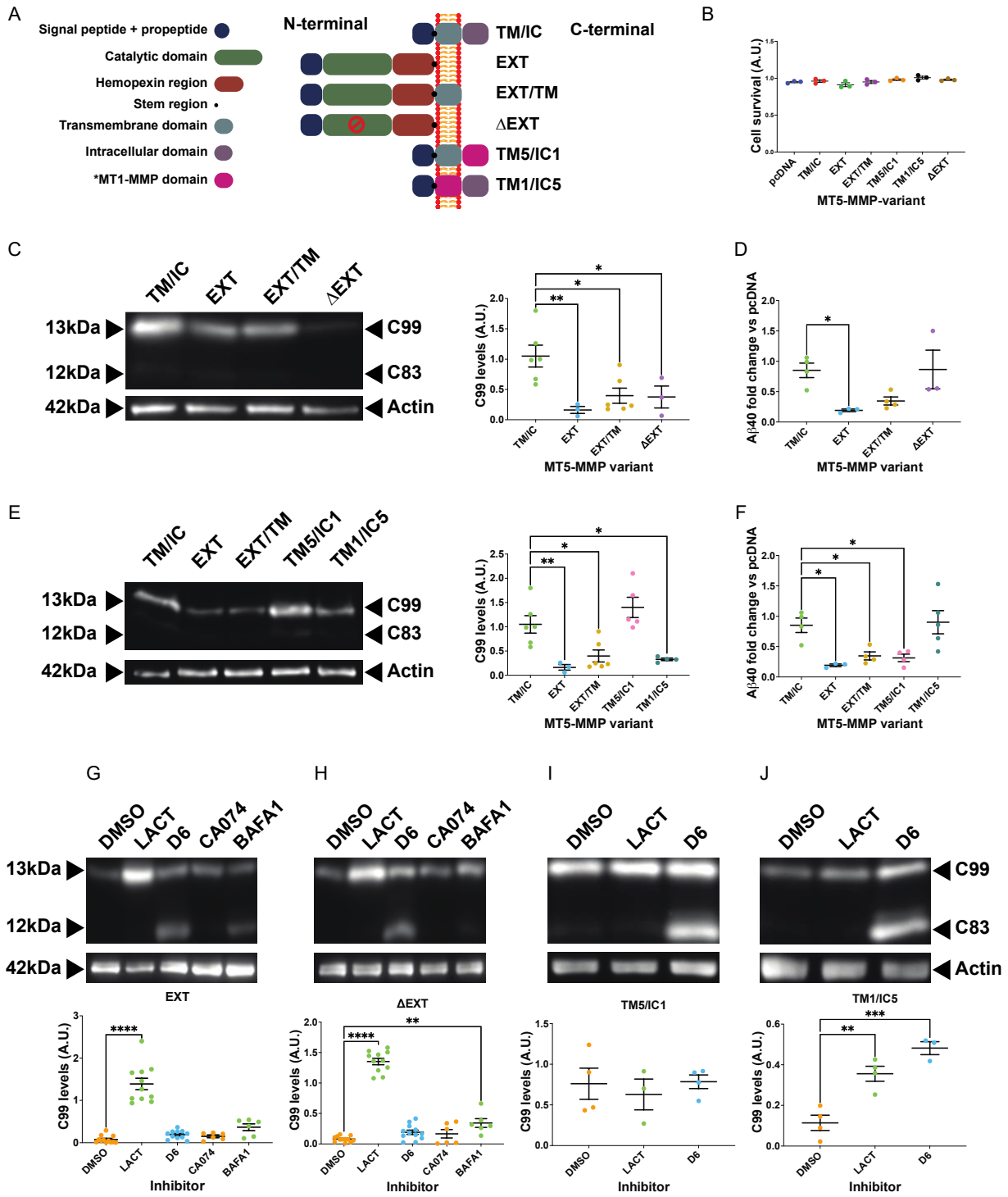

Figure 2.

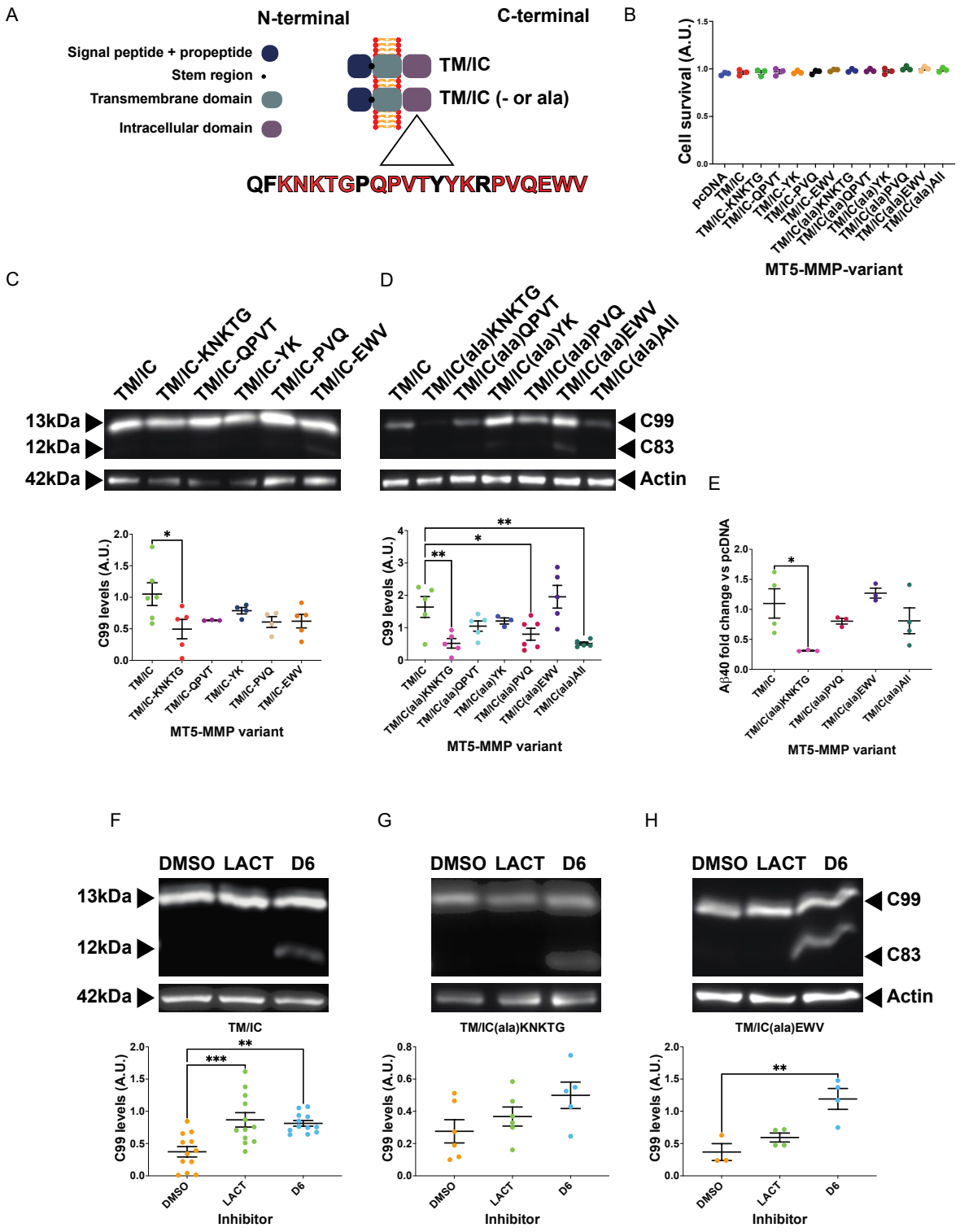
A
N-terminal
C-terminal
Signal peptide + propeptide
Stem region
Transmembrane domain
Intracellular domain
TM/IC
TM/IC (- or ala)
QFKNKTGPQPVTYYKRPVQEWV
B
Cell survival (A.U.)
pcDNA
TM/IC
TM/IC-KNKTG
TM/IC-QPVT
TM/IC-YK
TM/IC-PVQ
TM/IC-EWV
TM/IC(ala)KNKTG
TM/IC(ala)QPVT
TM/IC(ala)YK
TM/IC(ala)PVQ
TM/IC(ala)EWV
TM/IC(ala)All
MT5-MMP-variant
C
13kDa
12kDa
42kDa
C99 levels (A.U.)
MT5-MMP variant
D
C99
C83
Actin
E
Aβ40 fold change vs pcDNA
F
DMSO LACT D6
TM/IC
Inhibitor
G
TM/IC(ala)KNKTG
H
TM/IC(ala)EWV

Figure 3.

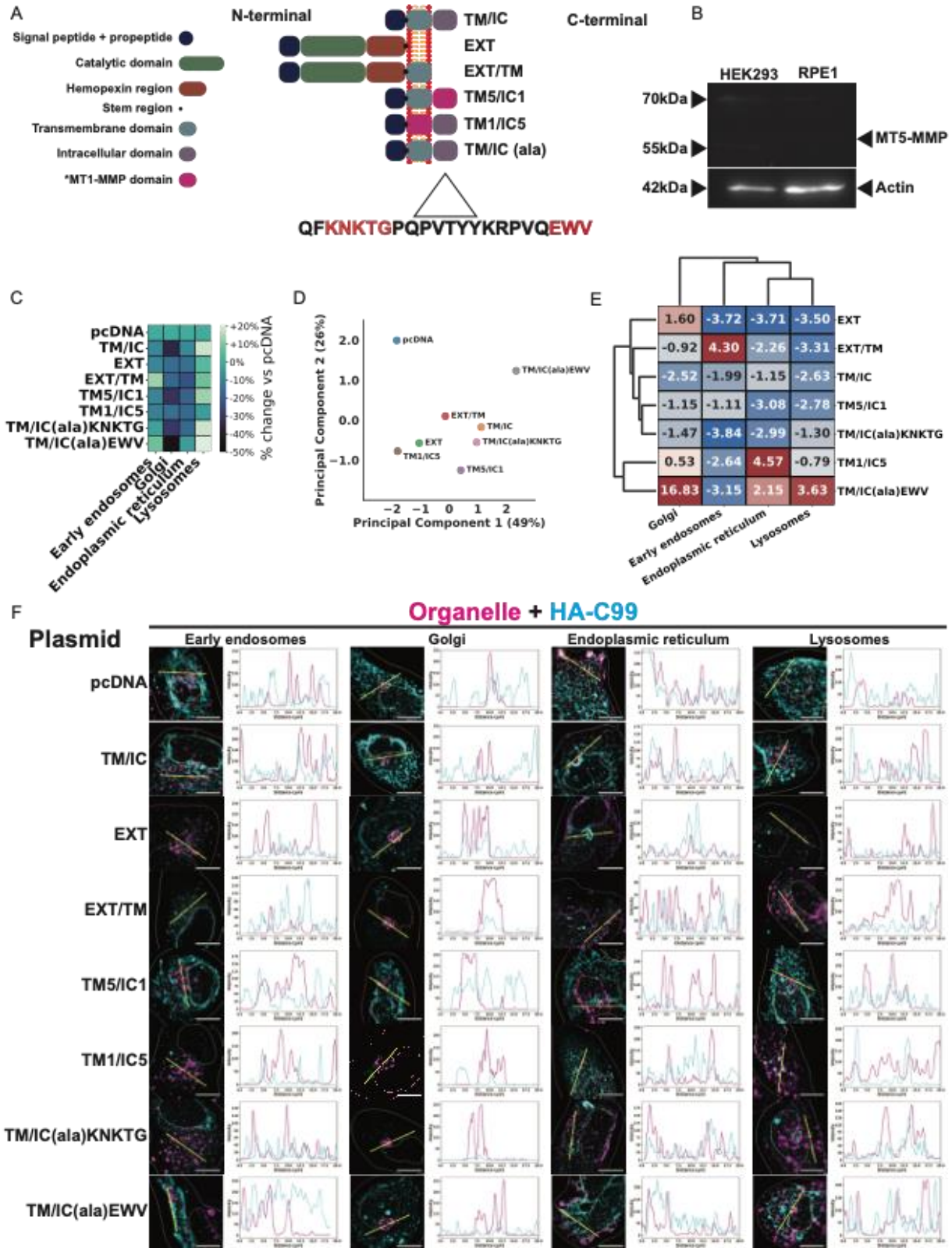
A
Signal peptide + propeptide
Catalytic domain
Hemopexin region
Stem region
Transmembrane domain
Intracellular domain
*MT1-MMP domain
N-terminal
C-terminal
TM/IC
EXT
EXT/TM
TM5/IC1
TM1/IC5
TM/IC (ala)
QFKNKTGPQPVTYYKRPVQEWV
B
HEK293
RPE1
70kDa
55kDa
42kDa
MT5-MMP
Actin
C
pcDNA
TM/IC
EXT
EXT/TM
TM5/IC1
TM1/IC5
TM/IC(ala)KNKTG
TM/IC(ala)EWV
Early endosomes
Golgi
Endoplasmic reticulum
Lysosomes
% change vs pcDNA
+20%
+10%
0%
-10%
-20%
-30%
-40%
-50%
D
Principal Component 2 (26%)
Principal Component 1 (49%)
pcDNA
TM/IC(ala)EWV
EXT/TM
TM/IC
EXT
TM/IC(ala)KNKTG
TM1/IC5
TM5/IC1
E
1.60 -3.72 -3.71 -3.50 EXT
-0.92 4.30 -2.26 -3.31 EXT/TM
-2.52 -1.99 -1.15 -2.63 TM/IC
-1.15 -1.11 -3.08 -2.78 TM5/IC1
-1.47 -3.84 -2.99 -1.30 TM/IC(ala)KNKTG
0.53 -2.64 4.57 -0.79 TM1/IC5
16.83 -3.15 2.15 3.63 TM/IC(ala)EWV
Golgi
Early endosomes
Endoplasmic reticulum
Lysosomes
F
Organelle + HA-C99
Plasmid
Early endosomes
Golgi
Endoplasmic reticulum
Lysosomes
pcDNA
TM/IC
EXT
EXT/TM
TM5/IC1
TM1/IC5
TM/IC(ala)KNKTG
TM/IC(ala)EWV

Figure 4.

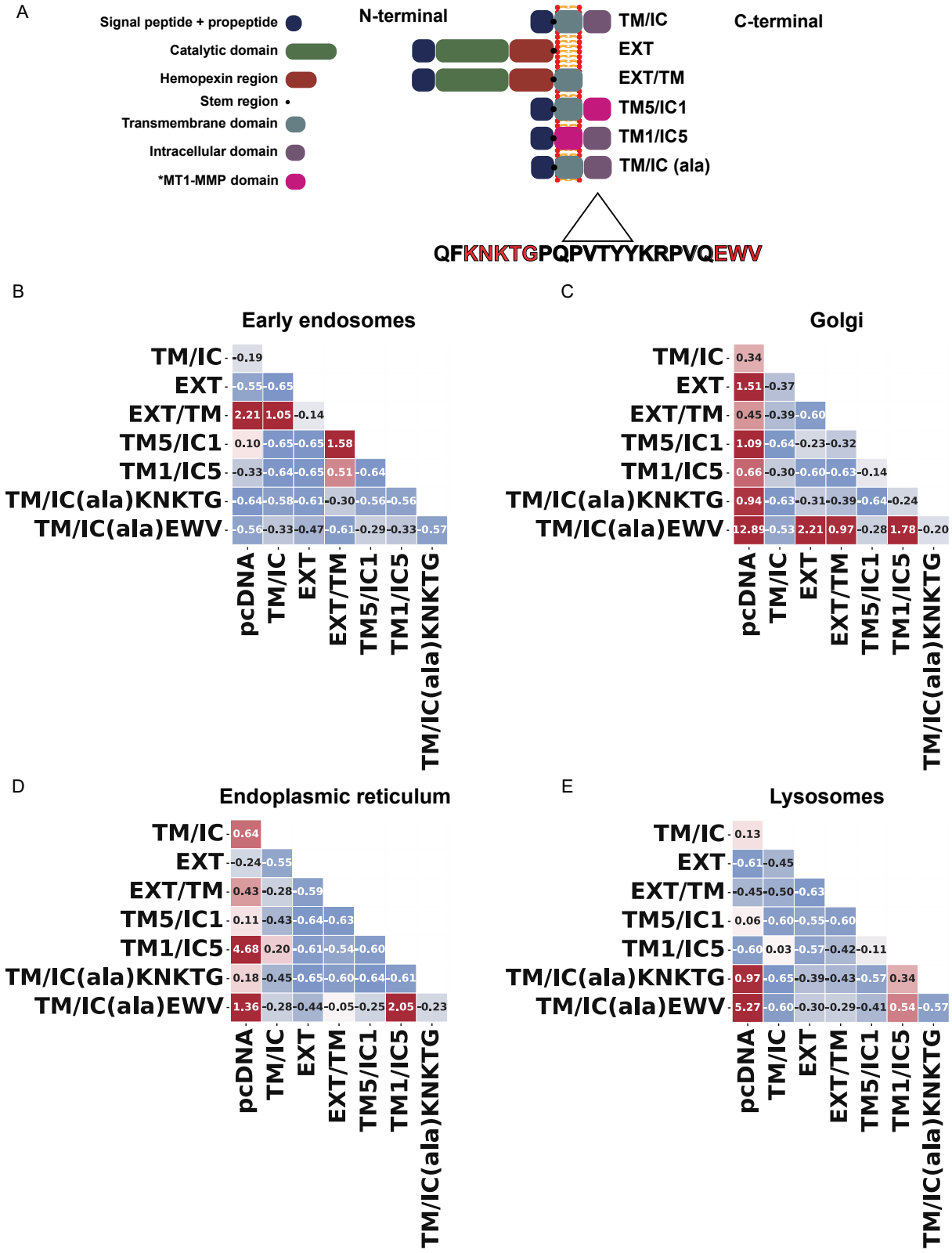
A
Signal peptide + propeptide
Catalytic domain
Hemopexin region
Stem region
Transmembrane domain
Intracellular domain
*MT1-MMP domain
N-terminal
C-terminal
TM/IC
EXT
EXT/TM
TM5/IC1
TM1/IC5
TM/IC (ala)
QFKNKTGPQPVTYYKRPVQEWV
B
Early endosomes
C
Golgi
D
Endoplasmic reticulum
E
Lysosomes
TM/IC
EXT
EXT/TM
TM5/IC1
TM1/IC5
TM/IC(ala)KNKTG
TM/IC(ala)EWV
pcDNA

Figure 5.

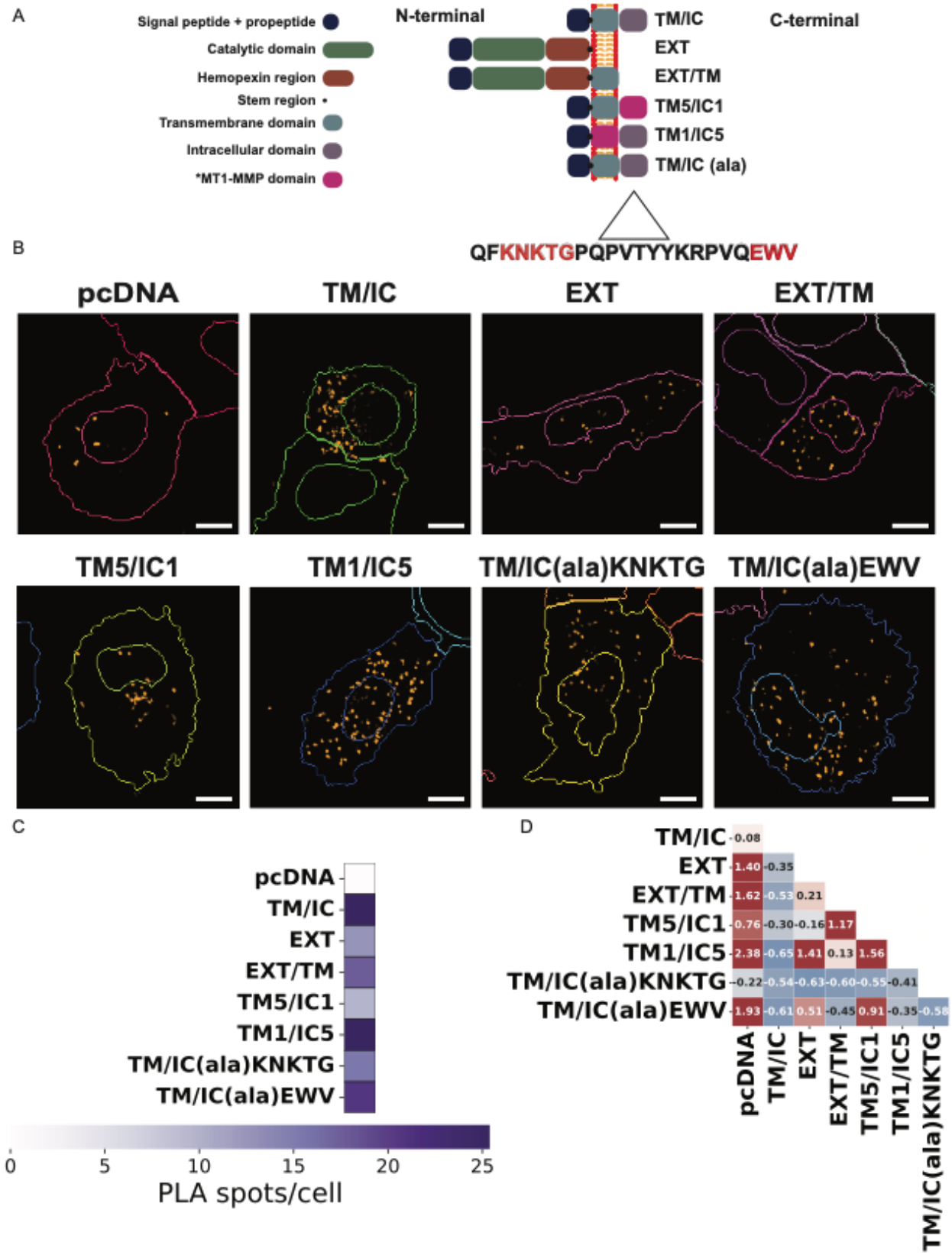
A
Signal peptide + propeptide
Catalytic domain
Hemopexin region
Stem region
Transmembrane domain
Intracellular domain
*MT1-MMP domain
N-terminal
C-terminal
TM/IC
EXT
EXT/TM
TM5/IC1
TM1/IC5
TM/IC (ala)
QFKNKTGPQPVTYYKRPVQEWV
B
pcDNA
TM/IC
EXT
EXT/TM
TM5/IC1
TM1/IC5
TM/IC(ala)KNKTG
TM/IC(ala)EWV
C
pcDNA
TM/IC
EXT
EXT/TM
TM5/IC1
TM1/IC5
TM/IC(ala)KNKTG
TM/IC(ala)EWV
0
5
10
15
20
25
PLA spots/cell
D
TM/IC -0.08
EXT 1.40 -0.35
EXT/TM 1.62 -0.53 0.21
TM5/IC1 0.76 -0.30 -0.16 1.17
TM1/IC5 2.38 -0.65 1.41 0.13 1.56
TM/IC(ala)KNKTG -0.22 -0.54 -0.63 -0.60 -0.55 -0.41
TM/IC(ala)EWV 1.93 -0.61 0.51 -0.45 0.91 -0.35 -0.58
pcDNA
TM/IC
EXT
EXT/TM
TM5/IC1
TM1/IC5
TM/IC(ala)KNKTG

Figure 6.

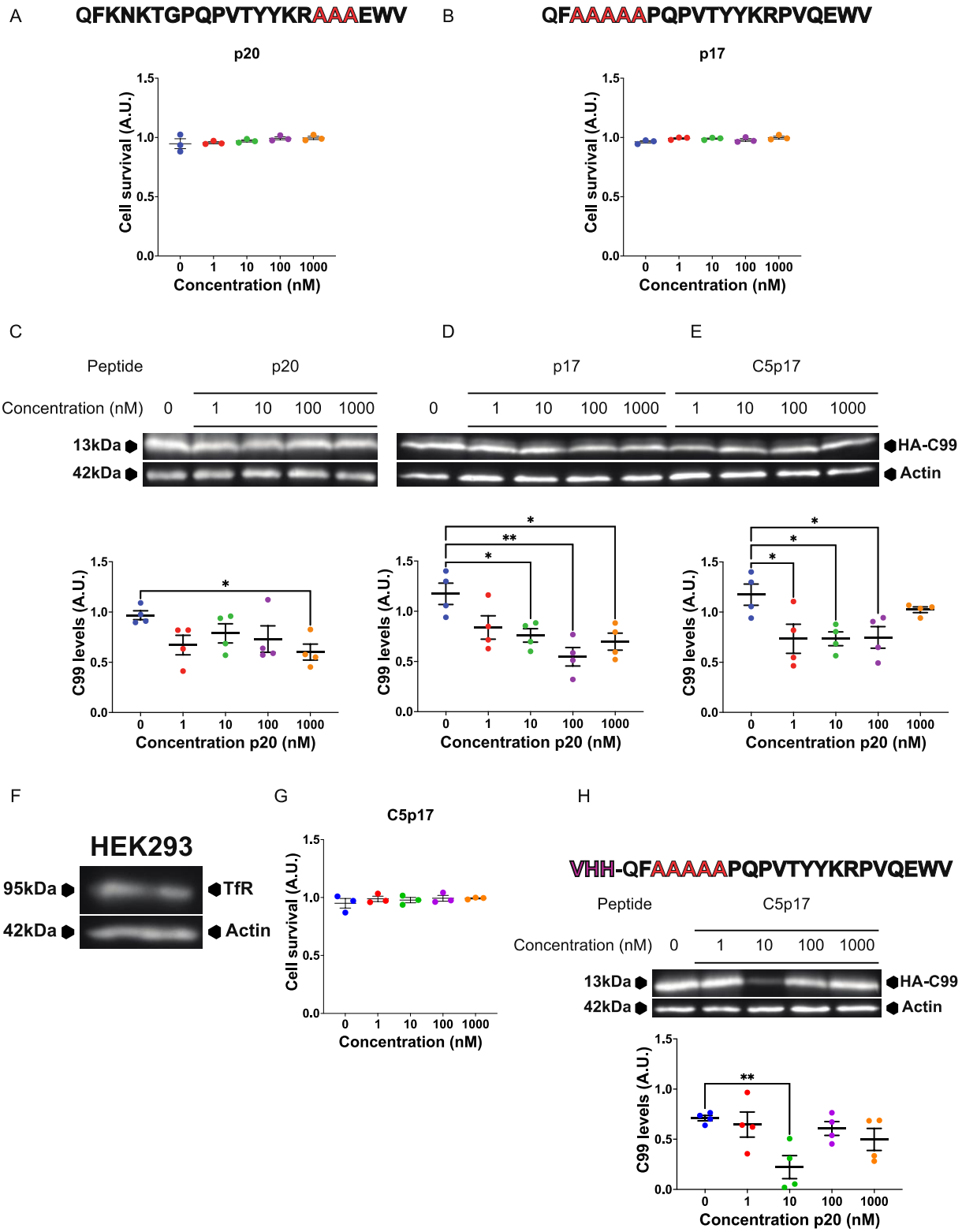
A
QFKNKTGPQPVTYYKRAAAEWV
p20
Cell survival (A.U.)
Concentration (nM)
B
QFAAAAAPQPVTYYKRPVQEWV
p17
Cell survival (A.U.)
Concentration (nM)
C
Peptide
p20
Concentration (nM)
13kDa
42kDa
C99 levels (A.U.)
Concentration p20 (nM)
D
p17
HA-C99
Actin
E
C5p17
F
HEK293
95kDa
42kDa
TfR
Actin
G
C5p17
Cell survival (A.U.)
Concentration (nM)
H
VHH-QFAAAAAPQPVTYYKRPVQEWV
Peptide
C5p17
Concentration (nM)
13kDa
42kDa
HA-C99
Actin
C99 levels (A.U.)
Concentration p20 (nM)